Marine and Petroleum Geology 149 (2023) 106090

Contents lists available at ScienceDirect

Marine and Petroleum Geology

journal homepage: www.elsevier.com/locate/marpetgeo

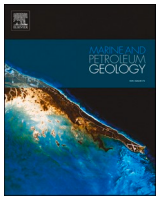

The influence of complex palaeobathymetry on development of deep-lacustrine fan systems

Darren J.R. Jones [a,*], Thomas J.H. Dodd [a,b], Dave J. McCarthy [a]

[a] British Geological Survey, The Lyell Centre, Research Avenue South, Edinburgh, EH14 4AP, UK
[b] Basin Dynamics Research Group, School of Geography, Geology and Environment, Keele University, Keele, Staffordshire, ST5 5BG, UK

ARTICLE INFO

Keywords:
Turbidite fans
Complex palaeo-bathymetry
Confinement
Deep-lacustrine
North Falkland Basin

ABSTRACT

Pre-existing complex palaeobathymetry often plays a key role in the spatial-temporal distribution and character of deepwater sedimentary systems. Particularly in deep-marine fan systems where their spatial-temporal association with complex syn-depositional palaeobathymetry have been widely investigated. When present in deep-marine settings, complex palaeobathymetry is known to affect flow-type, flow direction, and resultant fan distribution, which ultimately leads to atypical reservoir rock distribution. By contrast, far fewer studies explore the influencing controls of palaeobathymetry on deep-lacustrine sedimentary systems. This is important to investigate as deep-lacustrine basins have quite different allogenic and autogenic controls on flow types and resultant fan systems and fan lobes, which varies through different stages of basin configuration. To address this knowledge gap, this study documents and characterises a suite of deep-lacustrine sedimentary systems imaged in high-quality 3D seismic data from the rift-sag transitional and early post-rift phases of the North Falkland Basin, Falkland Islands. A range of multi-scalar seismo-geomorphological features are identified, including super systems, fan systems, fan lobes, and channel elements. The influence of palaeobathymetry on flows and resultant sedimentary features is evidenced by frontal and lateral structural confinement at the super system scale, and lateral confinement plus fan/flow deflection at the fan system, fan, and lobe scale. Offset stacking and compensational lobe-scale stacking geometries are developed in response to the type and scale of confinement. Palaeobathymetry, created as depositional relief by preceding fan deposits, is shown to progressively influence flow types and resultant spatial distribution of ensuing sedimentary systems. During periods of basin-fill where encircling palaeobathymetry ultimately controlled super system scale distribution, the ponding of flows and resultant fan features against intra-basinal highs formed thick packages of potentially coarse-grained sediments. As the basin filled-up and encircling topography exerted less control on super system scale distribution, flows were able to surmount the intra-basinal highs, leading to flow stripping processes. The combination of ponding and flow stripping processes resulted in the deposition and preservation of coarse-grained sediments immediately behind or on top of intra-basin structures. The results of this study provide key insights into the interaction of deep-lacustrine sedimentary systems and complex palaeobathymetry, which ultimately influences reservoir distribution.

1. Introduction

Confined and partly confined deepwater sedimentary systems are an important topic in siliciclastic sedimentary research (Winker, 1996; Prather et al., 1998; Lomas and Joseph, 2004; Cunha et al., 2017; Bell et al., 2018; Tagliaferri et al., 2018; Soutter et al., 2019). These systems form in a range of basin settings, including foreland basins (Kneller and McCaffrey, 1999; Mutti et al., 2009; Bayliss and Pickering, 2015; Tinterri and Tagliaferri, 2015), subduction zones (Pickering et al., 1992), passive margins (Prather, 2003; Adeogba et al., 2005; Albertão et al., 2011; Oluboyo et al., 2014), and rift basins or extensional settings (Gervais et al., 2004; Covault and Romans, 2009). Several distinct types of confinement exist, with a wide variety of classification systems. Deepwater systems can be 'unconfined,' (Shanmugam and Moiola, 1988; Normark et al., 1993; Lee et al., 1996; Posamentier and Kolla, 2003; Haughton et al., 2003; Fildani and Normark, 2004; Hodgson, 2009; Brunt et al., 2013) or 'confined' (Winker, 1996; McCaffrey and Kneller, 2001; Sinclair and Tomasso, 2002; Lomas and Joseph, 2004;

* Corresponding author.
E-mail address: darjones@bgs.ac.uk (D.J.R. Jones).

https://doi.org/10.1016/j.marpetgeo.2022.106090
Received 10 September 2022; Received in revised form 18 December 2022; Accepted 25 December 2022
Available online 26 December 2022

Covault and Romans, 2009; Marini et al., 2016a,b; Cunha et al., 2017; Tokes and Patacci, 2018). Other schemes recognise 'confined and contained,' 'confined and uncontained,' and 'unconfined and uncontained' categories (Smith, 1995; Southern et al., 2015). Confinement is multi-scalar, occurring at the basin scale, super system scale (multiple fan systems; Booth et al., 2003; Gervais et al., 2004; Li et al., 2010; Southern et al., 2015), through to the individual flow scale (Pickering and Hilton, 1998; Sinclair, 2000; Haughton, 2000; Sinclair and Tomasso, 2002; Amy et al., 2004; Gervais et al., 2004; Hodgson and Haughton, 2004; Smith and Joseph, 2004; Amy et al., 2007; Bersezio et al., 2009; As et al., 2010; Etienne et al., 2012; Yan and Kim, 2014; Marini et al., 2015; Spychala et al., 2017; Dodd et al., 2019). Pre-existing palaeobathymetry can influence flow pathways of turbidity currents, thereby providing control upon the loci of coarse-grained deposition in sedimentary basins (Gee *et al.*, 2001).

The sedimentary products of confined or ponded deepwater systems contrast with their less confined or unconfined counterparts (*sensu* Soutter et al., 2019). Ponded systems are shown to comprise more sheet-like depositional elements, and these are susceptible to mud-cap deposition and preservation (Fonnesu et al., 2016, 2018; Haughton et al., 2009; Talling, 2013; Patacci et al., 2014, 2020; Marini et al., 2016a,b; Southern et al., 2017; Tokes and Patacci., 2018). This contrasts with deposits formed within unconfined fan settings, which tend to be heterogeneous and more likely to form sand-prone channelised systems (Brunt et al., 2013; Lomas and Joseph, 2004; Terlaky and Arnott, 2016; Fallgatter et al., 2019). Sedimentary deposits formed under the influence of both frontal and lateral confinement have been modelled experimentally (Simpson, 1987; Al Ja'Aidi et al., 2004; Amy et al., 2004; Baas et al., 2004; Hamilton et al., 2017; Dorrell et al., 2018; Soutter et al., 2021). The effects of basin confinement upon the contained sedimentary systems fundamentally influences the character of the sediments deposited within them (Mutti and Normark, 1987; Amy and Talling, 2006; Davies et al., 2009; Kane et al., 2010; Straub and Pyles, 2012; Southern et al., 2014; Spychala et al., 2017; Soutter et al., 2019). Deepwater fan systems are known to form good-quality clast reservoir lithologies, which are particularly attractive when they drape over structural features (Drinkwater and Pickering, 2001; Gardiner, 2006; Chen et al., 2009; Li et al., 2014). Therefore, the effects of confinement on sedimentary systems are important to consider when exploring for conventional clastic reservoirs within deepwater petroleum systems (McCaffrey and Kneller, 2001; Posamentier and Kolla, 2003; Zhang et al., 2015).

Previous studies have focussed on confined systems in deep-marine settings, and in-particular on structurally complex regions such as intra-slope, terraced, or stepped margins (Prather et al., 1998; McHargue et al., 2011; Moscardelli et al., 2012), and in diapiric settings (salt/mud diapirs; Winker, 1996; Prather et al., 1998; Hansen et al., 2017). In-contrast, comparatively few studies examine the effect of confinement on deep-lacustrine sedimentary systems, which typically form in rift and failed-rift basin settings (Scholz et al., 1990; Ravnas and Steel, 1998; Soreghan et al., 1999; Corella et al., 2016; Xian et al., 2018). In terraced settings, sand often becomes trapped within lows along terraced margins, which preserves the relict conduits of sedimentary channel systems that feed the basinally-located lobe-dominated areas (Stow and Johansson, 2000; Carvajal and Steel (2009); Jobe et al. (2017). The basin geometries and overall structural configurations within deep-lacustrine settings display multiple types and scales of confinement (Gawthorpe and Leeder, 2000; Zhang and Scholz, 2015; Chen et al., 2020). Furthermore, deep-lacustrine settings have a range of internal and external controls on sedimentation and accommodation space. Chiefly, they lack a sustained oceanic connection and are instead more influenced by precipitation plus evaporation related to local-regional climate. Additionally, as deep-lakes tend to form in association with rift tectonics, there is a dynamic interaction between the in-draining sedimentary systems and the influence of contemporaneous faulting and accommodation space generated (Soreghan et al., 1999; Xu et al., 2018; Dodd et al., 2019; Zhang et al., 2019; Sun et al., 2020).

To provide insights into the character and controls on palaeobathymetrically influenced deep-lacustrine fan systems, this study examines a suite of 3D seismic data from the Western Graben of the North Falkland Basin (NFB), Falkland Islands. The NFB represents an example of a rift-basin system, whose rift-sag transitional to early post-rift phase sedimentary fill comprises deep-lacustrine fan systems. Through this analysis, this study addresses the following key questions.

i. What are the key sedimentary units in the Western Graben of the NFB at the super system, fan system, and fan lobe scale?
ii. What are the key structural features and how did they influence sedimentation?
iii. What are the distribution and thickness trends of deep-lacustrine fan systems in the Western Graben?
iv. What are the key internal seismo-geomorphological architectures within confined deep-lacustrine fan systems and fan lobes?
v. What are the types and scales of confinement, and how does it influence observed internal seismic morphologies?

Deep-lacustrine fans form key reservoir facies in numerous basins worldwide, such as the Barmer Basin in India (Dolson et al., 2015; Chatterjee et al., 2019), the NFB (Richards et al., 2006; Williams, 2015; Dodd et al., 2019, 2022), and the Ordos Basin (Xian et al., 2018). Therefore, through answering these key questions this study contributes to the improved understanding of deep-lacustrine systems.

2. Geological setting

The NFB represent one of four Mesozoic-aged offshore sedimentary basins that surround the Falkland Islands (Fig. 1). The first phase of basin formation is thought to be related to the break-up of Gondwana, with rifting initiating in the mid-late Jurassic (Richards et al., 1996a, b; Richards and Hillier, 2000; Stanca et al., 2019), resulting in a series of NW-SE trending grabens collectively known as the Southern North Falkland Basin (SNFB; Lohr and Underhill, 2015). The central and northern parts of the NFB record a later phase of rifting during the late Jurassic to earliest Cretaceous, which formed a series of N–S trending grabens that bisect the earlier trend (Richards et al., 1996a, b; Bransden et al., 1999; Richardson and Underhill, 2002; Lohr and Underhill, 2015). The second rifting phase was followed by a thermal sag phase initiating in the Berriasian/Valanginian (Richards and Hillier, 2000). The environment of deposition throughout the sag phase was predominantly continental and deep-lacustrine until Albian-Cenomanian times, when the basin began to develop increasingly marine conditions (Richards et al., 1996a, 1996b; Richards and Fannin, 1997; Richards and Hillier, 2000).

The Eastern Graben forms as a deep half-graben, with a series of north-south trending faults that define its eastern margin (Richards et al., 1996a, b; Richards and Fannin, 1997; Richards and Hillier, 2000; Lohr and Underhill, 2015). These westward-dipping normal faults influenced sedimentation through the creation of accommodation space (Lohr and Underhill, 2015; Dodd et al., 2019; Plenderleith et al., 2022). The Eastern Graben has been the focus of hydrocarbon exploration efforts, with hydrocarbon discoveries within deep-lacustrine turbidite fans, including Sea Lion (Fig. 1), Casper, Beverley, and Zebedee (MacAulay, 2015; Williams, 2015; Dodd et al., 2019, 2022), as well as the fans of the Isobel Embayment (Plenderleith et al., 2022).

This study focusses on the Western Graben, which forms as a shallower depocenter located to the west of the Eastern Graben. The Western and Eastern grabens are separated by the Orca Ridge, which is a north-south trending intra-basinal high (Figs. 1 and 2). The Western Graben is *c.* 50 km wide and 200 km long N–S striking half-graben, containing *c.* 2–4 km of sedimentary fill. It displays an eastward-thickening asymmetric profile towards the Orca Ridge (Fig. 2) and a southerly-deepening and widening overall basin geometry (Fig. 1). The Western Graben

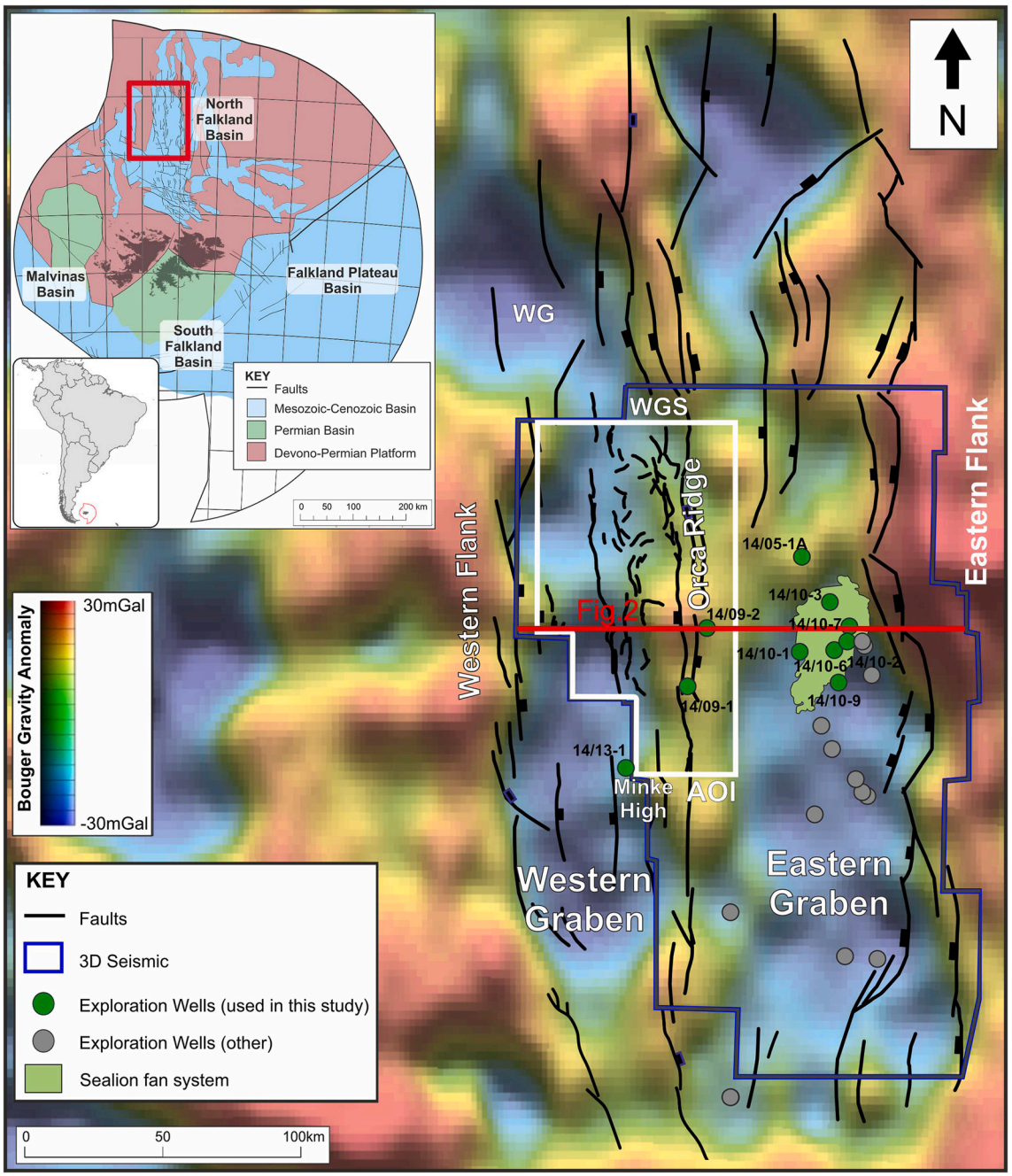

Fig. 1. The structural configuration of the North Falkland Basin, underlain by Bouguer gravity data. The area of interest for this study is highlighted by the white polygon. The blue polygon represents the extent of the merged 3D 'Company Composite' seismic volume. Modified fault lines are in black (from Richards et al. 1996b; Lohr and Underhill, 2015). Grey and green circles represent drilled exploration wells. The underlying Bouguer gravity anomaly map is filtered to wavelengths <100 km (data from Sandwell et al., 2014; modified from McCarthy et al., 2017). Top left inset image is a geological map of the offshore areas around the Falkland Islands (modified after Jones et al., 2019); the red box highlights the location of the main figure. WG: Western Graben; WGS: Western Graben Splay. (For interpretation of the references to colour in this figure legend, the reader is referred to the Web version of this article.)

exhibits large bounding faults at both its eastern and western margins, and shallows towards the west against the Western Flank basement high. The Western Graben branches into two shallower half-grabens in the north (the Western Graben and Western Graben Splay), which are separated by the northern continuation of the Orca Ridge (Jones et al., 2019). A pre-rift succession of likely Devonian-aged sediments was encountered in well 14/09-1 on the Orca Ridge (Richards and Hillier, 2000), which intersected a footwall to the main basin bounding fault.

Eight tectonostratigraphic units have been identified, including pre-rift, early syn-rift, late syn-rift, rift to sag transition, early post-rift, middle post-rift, late post-rift, and a post uplift sag phase (Richards and Hillier, 2000). The rift to sag transition, early post-rift, and middle post-rift are sub-divided into LC1–LC7 (Fig. 3; Richards and Hillier, 2000). Fluvio-lacustrine deposition was dominant in the early to late syn-rift, with a more-permanent lake developed during rift to sag transition to early post-rift times (Richards and Hillier, 2000). During the early post-rift, a southwards progradation of deltaic clinoforms, as well as concomitant margin-fed fan input into the lake (Richards et al., 2006; Williams, 2015; Dodd et al., 2019, 2022). A subsequent transgression resulted in the establishment of fluvio-lacustrine conditions by middle post-rift times, followed by marginal marine environments during the late post-rift, with permanent marine conditions developed in the Upper

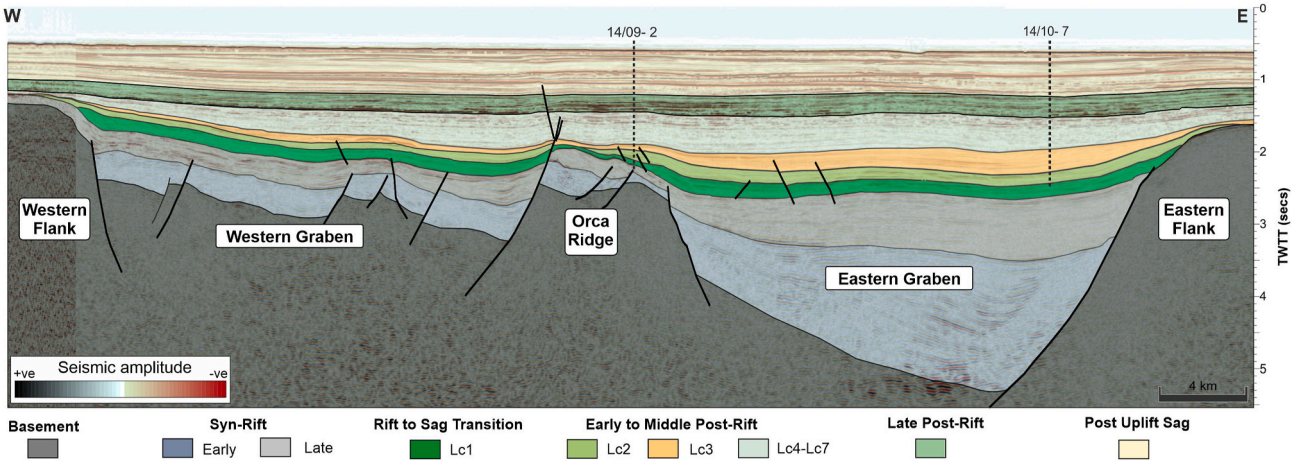

Fig. 2. A west-east oriented geoseismic section, including data from the merged 3D seismic volume, showing a typical cross-section profile both the Eastern and Western grabens of the North Falkland Basin. The section is sub-divided into eight coloured packages, which represent the main tectono-stratigraphic sub-units, as illustrated in the stratigraphic chart (Fig. 3), as well as the basement. Contains seismic data © Falkland Islands Government. All rights reserved.

Cretaceous. An ensuing period of Palaeogene regional uplift was followed by second thermal sag phase during the Cenozoic and associated deposition of marine and deltaic sediments (Richards and Hillier, 2000).

3. Methods and datasets

3.1. Well data analysis and correlation

Little well data exists from the Western Graben, with well 14/13-1 located on the Minke High to the south of the study area representing the only well to intersects the upper part (early post-rift) of the stratigraphy (Fig. 1). This well targeted a tilted fault block and encountered a thin post-rift section, which can be correlated over the Orca Ridge into the Eastern Graben. Nearby wells 14/09-1 and 14/09-2 were drilled the Orca Ridge to the east of the Western Graben (Fig. 1). Consequently, most of the known stratigraphy included in this study is constrained using well information and interpreted stratigraphical markers correlated from a suite of wells drilled in the Eastern Graben, and in-particular those around the Sea Lion area (Fig. 1). Several of these wells cored the Sea Lion Fan, providing significant geological insight into post-rift basin stratigraphy and the geology of these potentially analogous deep-lacustrine turbidite fan deposits (Williams, 2015; Dodd et al., 2019; Dodd et al., 2020; Dodd et al., 2022).

3.2. Seismic interpretation

This study utilises >4500 km^2 of full-stack 3D seismic reflection data, which consists of several merged seismic surveys acquired between 2007 and 2011 (Fig. 1). The volume underwent Kirchhoff pre-stack time migration, spectral whitening processing, and is displayed as zero phased to European (SEG reversed) polarity. This 3D volume displays high-quality, laterally continuous, seismically-bright reflectors down to *c.* 3.5 s two-way-travel time (TWTT), below which data quality reduces (Fig. 2).

The seismic interpretation workflow focussed on identifying the main faults and developing a structural framework for the Western Graben. Regional reflectors were identified across the NFB (Figs. 2 and 3) and were tied to existing wells in the Eastern Graben. Five seismic horizons were mapped, including 'Base LC1', 'Top LC1', 'Top LC2', 'Intra LC3' and 'Top LC3', which define the rift to sag transition and early post-rift packages (Fig. 3).

Previous studies using the same 3D seismic volume in the Eastern Graben interpreted increases in acoustic impedance (peaks) as representing sandstone-prone lithologies at the depth of the reservoir interval (Bunt, 2015). However, a reversal in top sandstone reflection polarity was identified at shallower levels of 1.2–2.2s TWTT, related to a transition from soft to hard impedance (Bunt, 2015). Consequently, as much of rift to sag transition and early post-rift in the Western Graben is within the window between 1.5 and 2.5s TWTT (Fig. 2), seismic picks have been made on troughs, with the seismically-brighter areas interpreted as representing potential sandstone-prone regions. An exception is made for the 'Base LC1' horizon, which is largely below 2.2s TWTT and is therefore interpreted as a peak. The seismic mapping led to the identification of basin depocentres and basin highs within the Western Graben (Figs. 4–13). Three additional horizons above the zone of interest were mapped regionally to permit depth conversion.

Horizons were gridded into surfaces at 50 m increments. Averaged interval velocities were applied between each surface, which were obtained from vertical seismic profiles in nearby wells (Fig. 1), creating a layer-cake velocity model for depth converting the time structure surfaces. Isopach maps were generated for the LC1, LC2, lower LC3, and upper LC3 intervals (Fig. 4).

3.3. Seismic attribute analysis: amplitude, variance, and spectral decomposition

Two types of amplitude extraction were performed: maximum amplitude, which measures the largest positive reflectivity within a time window; and Root Mean Squared (RMS) amplitude, which calculates the largest average value of amplitude reflectivity. Changes in response to seismic amplitude can be related to variations in lithology or fluid-fill in the subsurface (Chopra and Marfurt, 2005). On this basis, a general assumption is made that higher amplitudes represent sand-rich bodies, whilst lower amplitudes represent more mudstone-rich intervals. This study assumes that the amplitude variations observed are a function largely of rock type but acknowledges that they may also be affected by variations in fluid-fill or by thin-bed tuning effects. On this basis, the resultant maps were used for the identification and mapping of potential sedimentary systems. Scales of mapped sedimentary system include super system, fan system, fan lobe, and channel elements (Fig. 5).

The variance attribute was calculated and used to identify discontinuities in the dataset at the mapped horizons. This attribute measures the continuity between seismic traces along a picked horizon and has been used to highlight fault trends, basins, highs, channel systems, and fan geometries. Variance and amplitude extractions were applied to time windows (0–200 ms) and horizon time-offsets for each key horizon interval.

Spectral decomposition (or 'time-frequency analysis'; Farfour et al.,

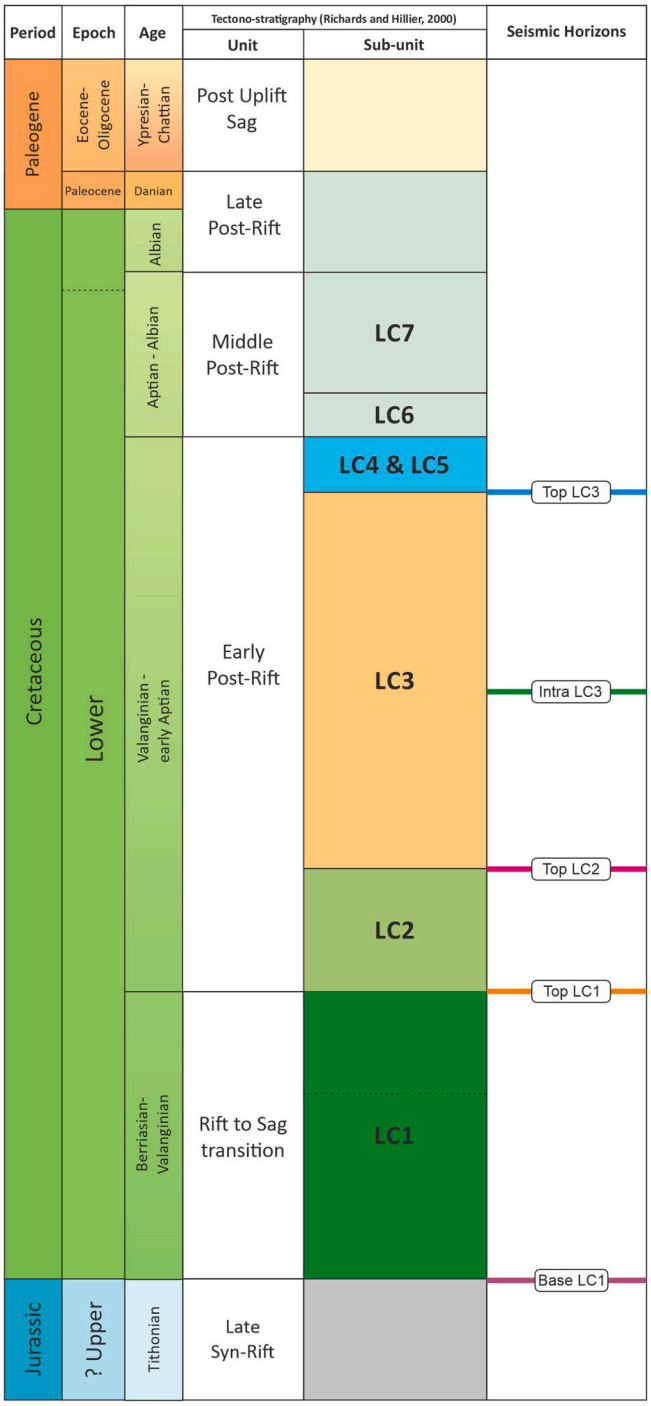

Fig. 3. A tectono-stratigraphic chart for the North Falkland Basin, ranging from the Jurassic to the Palaeogene. Nomenclature for these packages has been taken from Richards and Hillier (2000). Note 'LC' stands for 'Lower Cretaceous.' A comparison of the interpreted horizons and stratigraphy in this study, with the tectono-stratigraphic units as defined in Richards and Hillier (2000) is provided.

2017) was performed on this dataset. Combinations of frequency-dependent 'red-green-blue' (RGB) blends were trialled, with optimal viewing conditions at 15-25-30 Hz. Resultant 'RGB maps' were displayed in a 3D cube for geo-body evaluation.

3.4. Analogue fan systems

The Eastern Flank deep-lacustrine fan systems of Sea Lion North, Sea Lion, Otter (Williams, 2015; Dodd et al., 2019), Beverley, Casper, Zebedee (Bunt, 2015; Francis et al., 2015; Dodd et al., 2022), and systems of the Isobel Embayment (Plenderleith et al., 2022) form comparable and potentially contrasting fan analogues for the systems described in this study. The Eastern Flank systems are characterised by high amplitude seismic reflectors, which form a range of fan system types, with a wide range of recognisable internal seismic architectures (*sensu* Dodd et al., 2019; Dodd et al., 2022). These fan systems display abrupt lateral and distal pinch-outs.

4. Results

4.1. Base LC1 (top late syn-rift)

4.1.1. Description

At the base LC1 horizon, the Western Graben (Fig. 6a) consists of four separate depocentres, termed 'depocentre 1–4'. In the south, depocentre 1 forms the deepest part of the Western Graben, reaching a maximum depth of 2600 m. Depocentre 1 is separated from depocentre 2 to the west by a basin high. Depocentre 2 is the shallowest, with a maximum depth of 2300 m. To the north, depocentres 3 and 4 deepen to 2450 m and 2550 m, respectively. They are separated by a basin high related to a northern splay of the Orca Ridge.

The margins of the Western Graben shallow upwards to 1300 m over the Western Flank, and 2000 m over the Orca Ridge. A series of N–S/NW-SE oriented faults define the western and eastern edges of the Western Graben. In relation to this N–S/NW-SE trend, a series of parallel to sub-parallel intra-basinal faults are visible in the variance data (Fig. 6b). Additionally, secondary fault sets and other non-fault-related discontinuities are visible, displaying NE-SW and E-W orientations.

A maximum amplitude extraction on a 10 ms window, with zero offset of the Base LC1 horizon, shows regional sedimentary systems preserved at the base of LC1 (see Fig. 6c). Western areas are dominated by west-east oriented elongate high amplitude features, with a branching network of sinuous and linear channel-like features (<500 m in width), which are surrounded by low amplitude areas. As the systems move easterly into the depocentres, the high amplitude features gradually widen, forming lobate geometries. Multiple fanning-outwards geometries in the west appear to coalesce in the various depocentres in the east, with fewer intervening low amplitude areas.

4.1.2. Interpretation

A series of broadly west-east flowing deep-lacustrine super systems, fan systems, and lobes are interpreted in the Western Graben at this stratigraphic level. Discontinuities in the variance maps (Fig. 6b) are interpreted as large-scale erosional scour features related to sinuous channels and canyon systems, through which sediment bypassed into the eastern areas of the Western Graben. Areas of high amplitudes have been mapped and separated into discrete fan systems, fan lobes, and channel elements (Fig. 6c), which have been grouped into five sedimentary super-systems termed S1–S5, moving from south-to-north (Fig. 6d; Table 1).

4.2. Top LC1 (rift to sag transition)

4.2.1. Description

The Top LC1 reflector is characterised by four separate depocentres that show a N–S elongated planform geometry (Fig. 7a). Depocentre 1 represents the deepest area at this stratigraphic interval, reaching *c.* 2400 m (Fig. 7a). It has a stratal thickness of *c.* 150 m (Fig. 4a) and is bound to the east and west by a series of N–S trending faults. Depocentre 2 is separated from depocentre 1 by a basin high, reaching depths of 2150 m (Fig. 7a) and has a stratal thickness of up to 150 m (Fig. 4a). Depocentre 2 shallows westward to 1400 m on the Western Flank. To the north-east, depocentre 3 is bordered by N–S oriented faults along the Western Flank and along the Orca Ridge to the east, where it deepens to

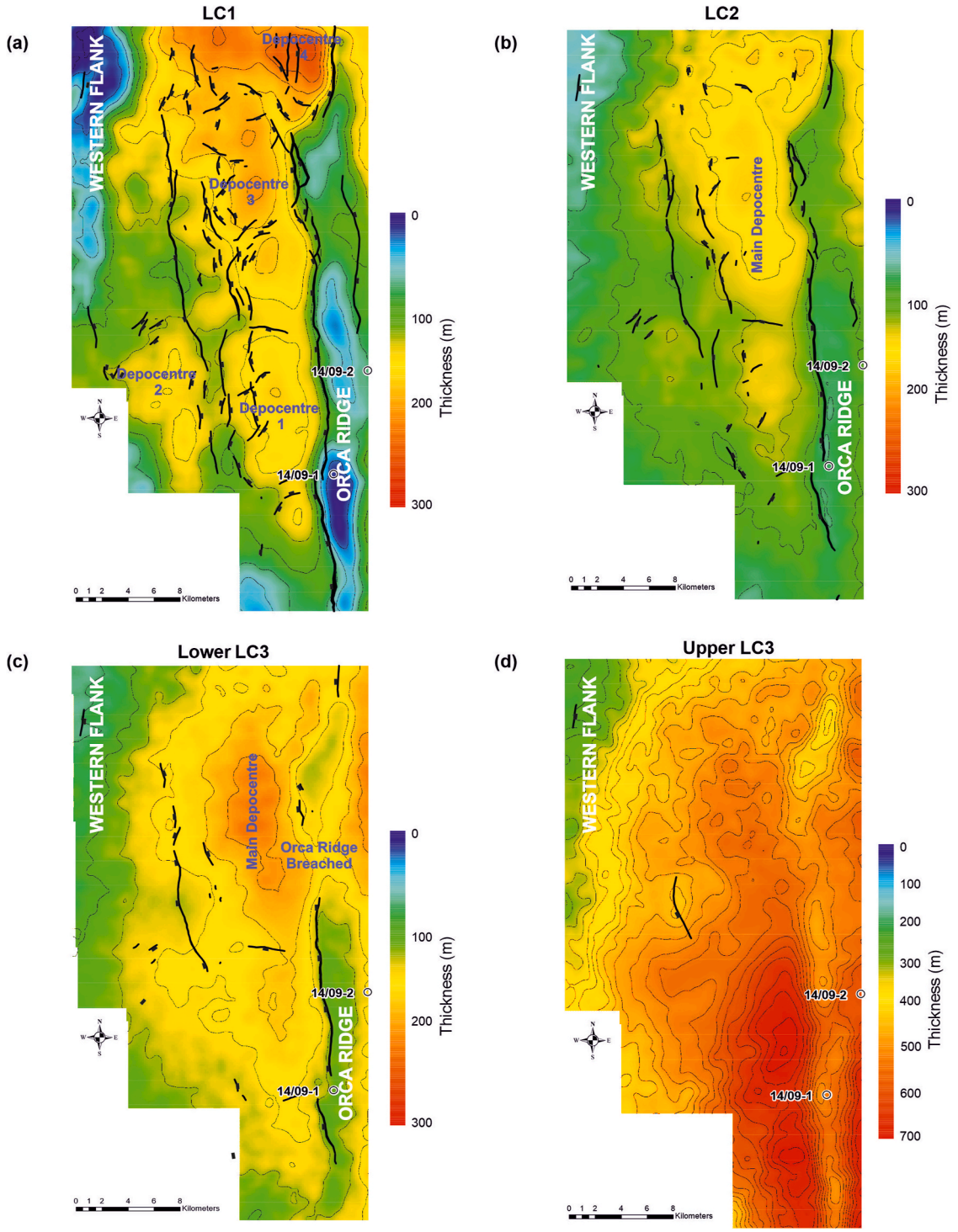

Fig. 4. Isopach thickness maps (in metres) for the rift-sag transition to early post-rift units across the Western Graben. Contours are spaced at 25 m intervals. The thick black lines represent faults that intersect each interval. (a) LC1. (b) LC2. (c) Lower LC3. (d) Upper LC3.

2330 m in the centre (Fig. 7a). Depocentre 3 has a thickness of up to 250 m (Fig. 4a).

An intra Orca Ridge structural low, or break, is observed directly east of depocentre 3, particularly in the variance slice where an area of low variance and along-strike discontinuities are present between northern and southern edges of the Orca Ridge (Fig. 7a and b). Depocentre 4 reaches depths of 2200 m (Fig. 7a) displays stratal thicknesses of *c.* 300 m (Fig. 4a), and is separated from depocentre 3 by a basin high. High amplitude features are widespread along the eastern margin of the Western Graben, adjacent to the Orca Ridge, whilst to the west high amplitudes are more spatially restricted and often characterised by elongate areas of high amplitude that are otherwise surrounded by areas of low seismic amplitude (Fig. 7c).

4.2.2. Interpretation

The high and low amplitudes observed at this interval have led to the identification of a series of fan systems, fan lobes, and channel elements (Fig. 7c), which have been grouped into five sedimentary super systems

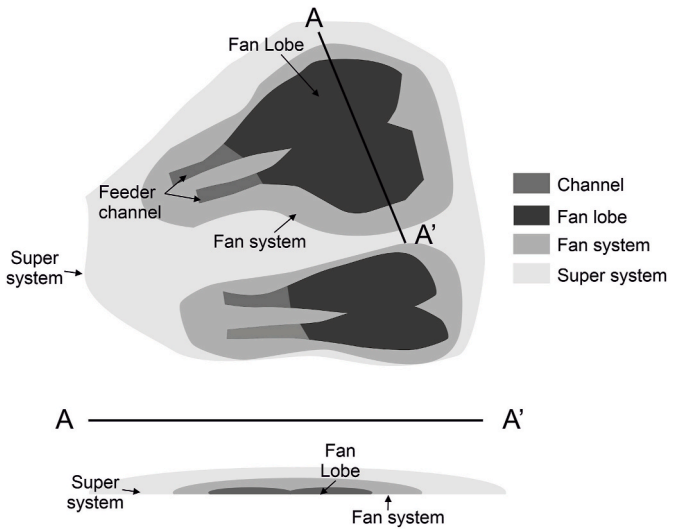

Fig. 5. Schematic diagram showing a hierarchical fan system classification scheme. A fan system is a distinct seismo-geomorphological feature imaged by 3D seismic data, which is fed by a single feeder system/channel, or closely spaced (e.g. 100s of meters) series of feeder systems/channels. Fan systems can be grouped into super systems, largely based on a common source area, similar or comparative aerial profiles/seismio-geomorphology, and chronological commonality (i.e., contemporaneous or penecontemporaenous systems form a super system). Lobe and channels form the principal internal components of fan systems, and form at a smaller scale. Lobe elements are defined as the internal architectures observed within lobes and are more-closely related to flow-scale processes.

termed S1–S5, moving from south-to-north (Fig. 7d; Table 2).

4.3. Top LC2 (lower early post-rift)

4.3.1. Description

At the LC2 stratigraphic interval, the Western Graben forms a single connected depocentre, which progressively deepens from 2100 m to 2300 m (Fig. 9a) and thickens from 150 to 200 m (Fig. 4b) moving from south to north. The eastern margin of the Western Graben is bound by a continuous system of N–S oriented faults, whilst to the west there is a more discrete set of generally smaller (in length) N–S faults that form the edge of the Western Flank.

Linear, W-E oriented discontinuities are visible on the variance attribute at this interval (Fig. 9b). In the east, a network of narrow, slightly sinuous architectures is surrounded by broader and laterally extensive lower amplitude areas (Fig. 9c). The narrow areas of higher amplitude progressively widen moving from west to east. The highest seismic amplitudes observed at this stratigraphic interval are in the northern-most and southern-most parts of the study area.

4.3.2. Interpretation

Some of the W-E oriented discontinuities observed in the variance maps (Fig. 9b) are associated with high amplitudes and therefore interpreted to be feeder channels (Fig. 9c and d) that traversed the western slope. These channels fed the lobe-dominated parts of the systems in the east, where variance attribute maps become more continuous. High amplitudes in the east are likely associated with numerous fan systems and internal lobes that coalesced and became frontally confined against the western edge of the Orca Ridge (Fig. 9c). These high amplitudes have been identified and grouped into four sedimentary super systems termed S1–S4, moving from south-to-north (Fig. 9d; Table 3).

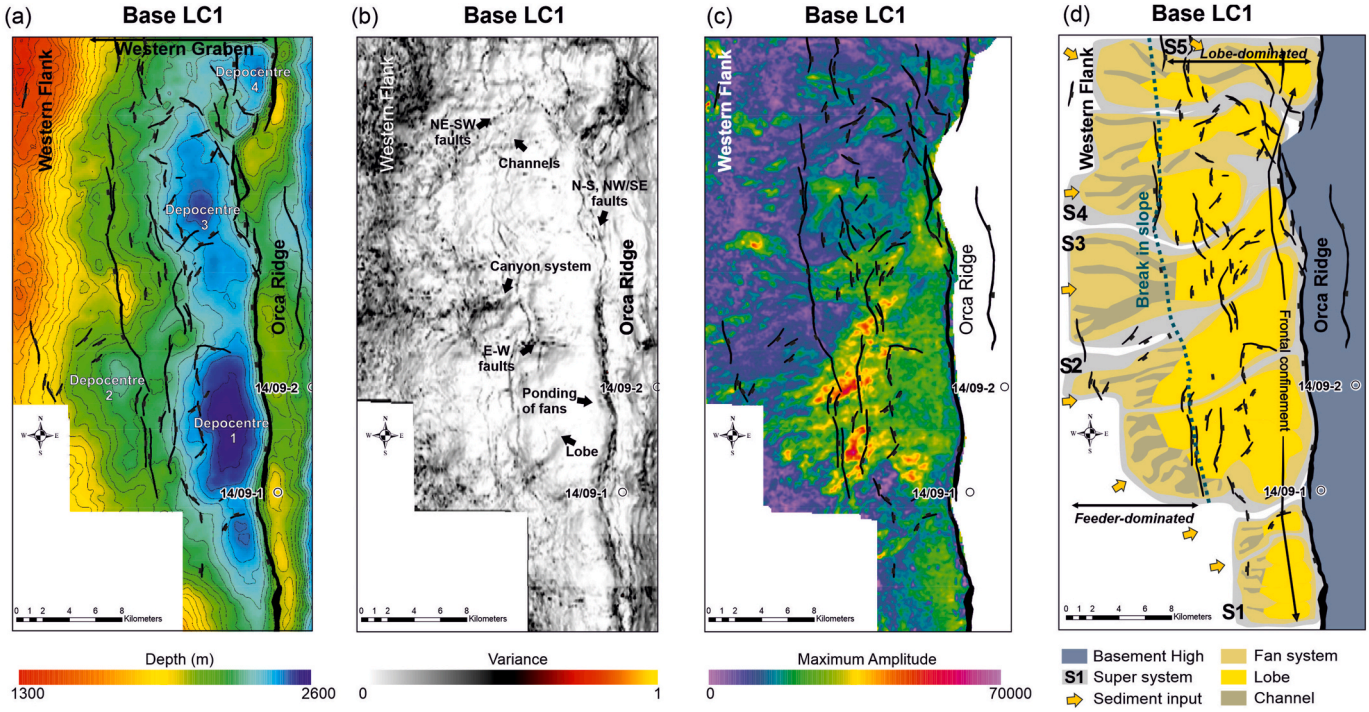

Fig. 6. Seismic characteristics of the Base LC1 horizon. (a) A depth-structure map of the Base LC1 horizon in the Western Graben, showing the four main depocentres labelled on the image. Contours are spaced at 25 m intervals. (b) A variance attribute map draped over the Base LC1 horizon. Discontinuities are shown in black and highlight the main structural features that intersect this surface. (c) A maximum amplitude extraction map produced from a 10 msec window, with zero offset from the mapped Base LC1 horizon, cropped at the western boundary of the Orca Ridge. Brighter colours indicate higher amplitude values that likely correspond to either sand bodies or fluid changes in the subsurface. Orange polygons represent interpreted fan systems, whilst yellow outlines demarcate individual channels and lobes. (d) An interpreted seismic facies map of the Base LC1 horizon, showing the super systems, fan systems, lobes, and channels. (For interpretation of the references to colour in this figure legend, the reader is referred to the Web version of this article.)

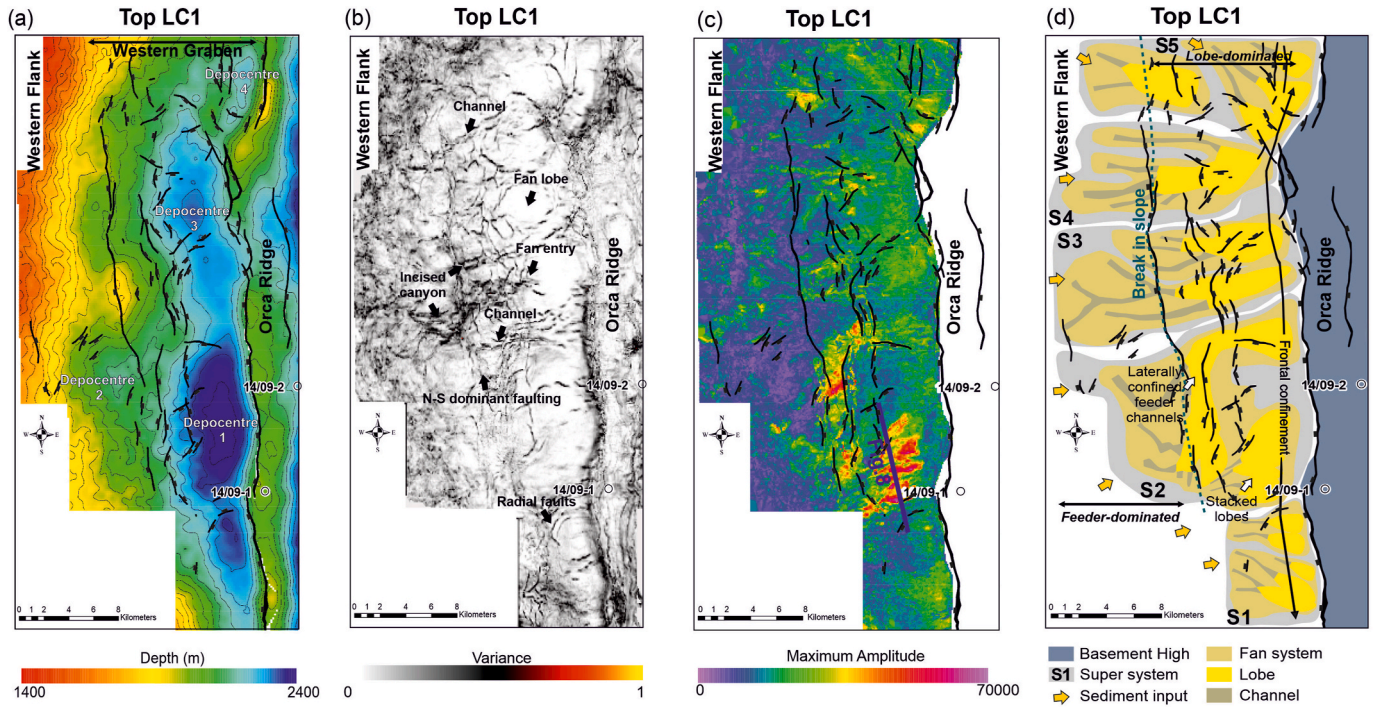

Fig. 7. Seismic characteristics of the Top LC1 interval. (a) A depth-structure map of the Top LC1 horizon in the Western Graben, showing the four main depocentres. Contours are spaced at 25 m intervals. (b) A variance attribute draped over the Top LC1 horizon. Discontinuities are shown in black, and which highlight the main structural features that intersect this interval. (c) Maximum amplitude extraction map of a 100 msec window, taken with a −20 msec offset from the Top LC1 horizon, cropped at the western boundary of the Orca Ridge. Brighter colours indicate higher amplitude values that likely correspond to either sand bodies or fluid changes in the subsurface. Orange polygons represent interpreted fan systems, whilst yellow outlines demarcate individual lobes and channels. Note cross-section through the fan system as shown in Fig. 8. (d) An interpreted seismic facies map at the Top LC1 horizon, showing the super systems, fan systems, lobes, and channels. It is characterised internally by northern and southern fan systems, composed of stacked lobes in the south, and laterally confined feeder channels in the north. (For interpretation of the references to colour in this figure legend, the reader is referred to the Web version of this article.)

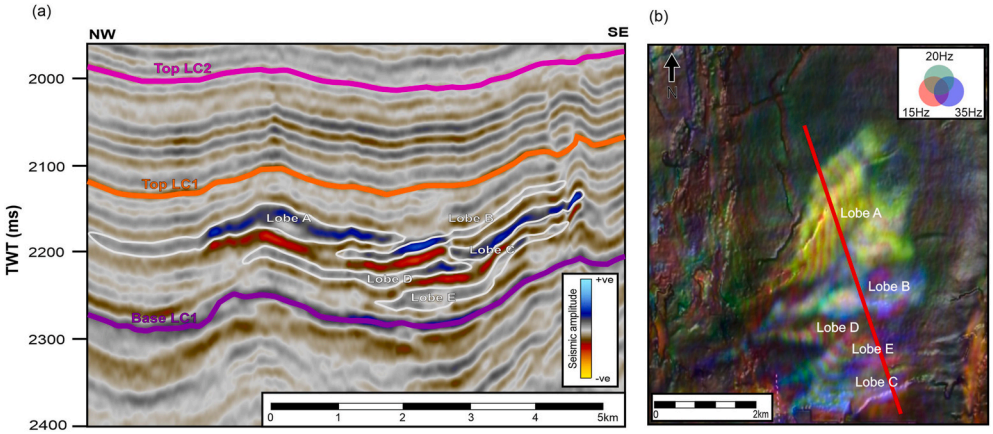

Fig. 8. (a) A NW-SE two-way-travel-time seismic section through the LC1 interval, showing the southern stacked geometry of super system 2. The main tectonostratigraphic units are displayed as coloured horizons, whilst the white outlines highlight the extent of the fan bodies. (b)Geometries and relationships of five stacked fan lobes using spectral decomposition (15-20-35 Hz RGB blend), with a 100 msec window and 50 msec offset above base LC1. Contains seismic data © Falkland Islands Government. All rights reserved.

4.4. Lower LC3 (early post-rift)

4.4.1. Description

Sedimentary systems during the Lower LC3 sub-unit are evaluated using an RMS amplitude extraction window (Fig. 10), created between the Top LC2 and Intra LC3 horizons. Three high amplitude areas are identified within the Western Graben during the Lower LC3 interval. In the southern-most part of the study area, an overall N–S oriented series of elongate or lensoidal, arcuate, high amplitude architectures are observed, displaying planform geometries that are quite different to other features in the Western Graben or the wider NFB (Fig. 10). In the middle part of the study area, a series of W-E oriented high amplitude features traverse across the Western Flank, extending down and into the Western Graben, past the Orca Ridge and into the Eastern Graben. In the northern part of the study area, N–S oriented high amplitude features are present. These amplitudes become brighter as they terminate against the W-E oriented high amplitudes (Fig. 10).

4.4.2. Interpretation

The three high amplitude areas identified in the south, central, and northern parts of the RMS extraction are interpreted as three separate depositional systems within the Western Graben during the Lower LC3 interval (Fig. 10). The arcuate or lensoidal shaped high amplitude architectures in the south are interpreted as a carbonate reef complex, as observed from hummocky high amplitude seismic geometries in cross-sectional view (Fig. 11).

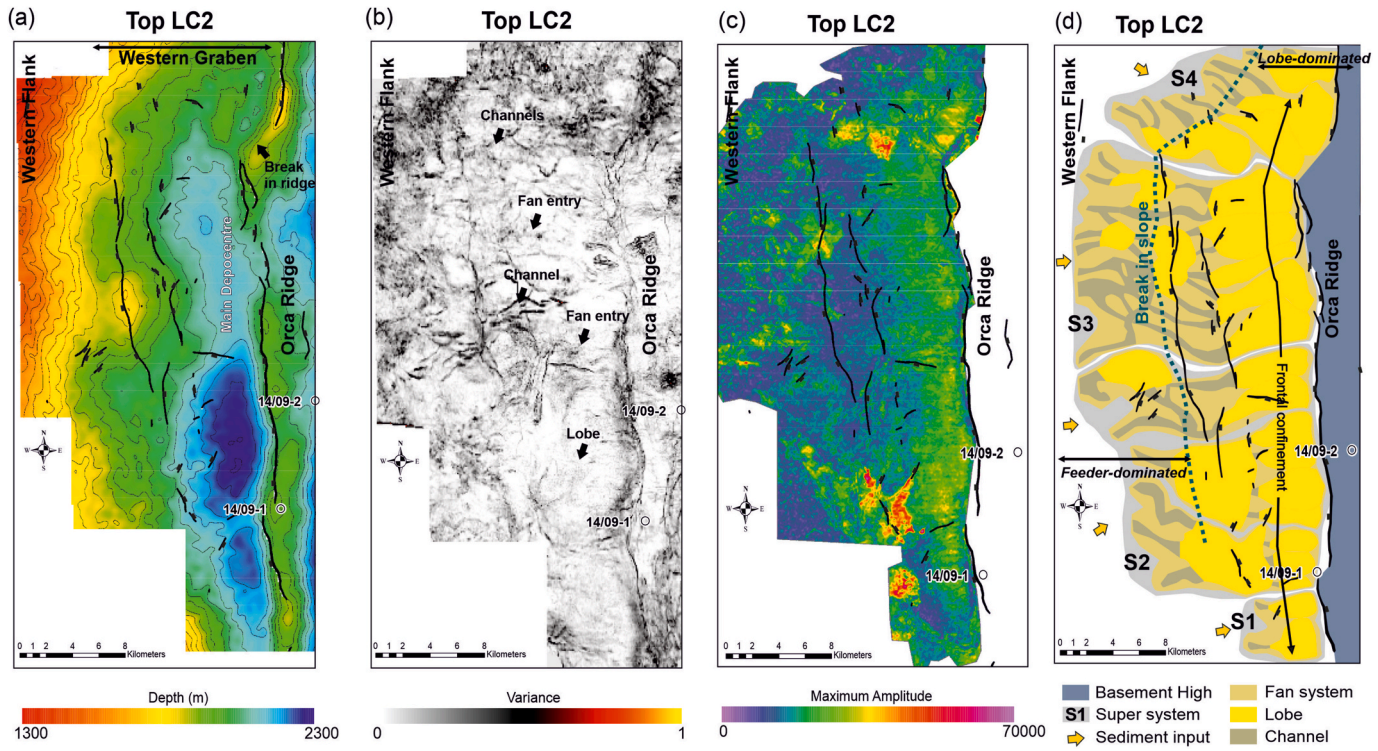

Fig. 9. Seismic characteristics of the Top LC2 interval. (a) A depth-structure map of the Top LC2 horizon in the Western Graben study area, showing a single main depocentre. Contours are spaced at 25 m intervals. (b) A variance attribute draped over the Top LC2 horizon, discontinuities are shown in black and highlight the main structural features at this interval. (c) Maximum amplitude extraction map taken from a 150 ms window, with zero offset on the Top LC2 horizon, cropped at the western boundary of the Orca Ridge. Brighter colours indicate higher amplitude values, which likely correspond to either sand bodies or fluid changes in the subsurface. Orange polygons represent fan systems, whilst yellow outlines demarcate individual lobes and channels. (d) Interpreted seismic facies map of the Top LC2 horizon, showing the super systems, fan systems, lobes, and channels. (For interpretation of the references to colour in this figure legend, the reader is referred to the Web version of this article.)

In the middle part of the study area, the W-E oriented high amplitude features represent a series of westerly-derived fan systems (Fig. 10). The flows that deposited the fan systems are interpreted to have travelled from the Western Flank, down into the Western Graben, where they were mostly frontally confined against the Orca Ridge. However, some of the flows overtopped the Orca Ridge or were diverted around its northern edge, transporting their sediments out and into the Eastern Graben. The Sea Lion North Fan is also observed at this stratigraphic level, as shown by the high amplitude features in the Eastern Graben (Fig. 10), suggesting that these systems were coeval. In the northern area, the N–S oriented linear features are interpreted as northerly-derived deltaic sediments that interacted with the westerly-derived fan systems. The linear edge along which they terminate is interpreted as the base of the distal prodelta deposits (Fig. 10).

4.5. Intra LC3 (early post-rift)

4.5.1. Description

A depth structure map of the Intra LC3 horizon illustrates that the Western Graben consisted of a single main depocentre (Fig. 12a). This depocentre was deepest directly adjacent to and along strike from the Orca Ridge, varying from *c.* 2200 m in the south to *c.* 2000 m in the north, thickening to a maximum of 300 m towards the centre of the graben (see Fig. 4c, where it has been referred to as lower LC3). N–S and NW-SE trending faults border the western margin of the Orca Ridge, with a number intersecting the Western Flank (Fig. 12b).

In the northern area, the variance data shows a series of sinuous N–S trending architectures (Fig. 12b), which can be correlated with discrete NE-SW oriented high amplitude features (Fig. 12c). By contrast, the variance slice in the central part of the graben shows a series of W-E oriented discontinuities (Fig. 12b), which can be correlated with a series of W-E oriented high amplitudes features across the Western Graben and Orca Ridge (Fig. 10c). In the central part of the graben, a cluster of high seismic amplitudes brighten from west to east (Fig. 12c). In the southern part of the study area, a series of arcuate or lensoidal high amplitude architectures are flanked to the east by moderately bright discontinuous amplitudes features (Fig. 12c). These features form hummocky seismic reflections, with down-lapping stepped profiles (Fig. 11). These features are located directly over a mid-basin high, with compactional drape observed above its edges (Fig. 11).

4.5.2. Interpretation

In the northern parts of this depocentre, the variance data illustrates a series of sinuous N–S trending features, which are interpreted as delta-top channels, marking a provenance change for the depositional systems in this part of the basin (Fig. 12b) associated with progradation of a northerly-derived delta (Fig. 12c and d). In contrast, the series of W-E oriented discontinuities (Fig. 12b) and high amplitudes of the central areas (Fig. 12c) represent a continuation of the eastwardly driven deep-lacustrine fan systems. Two sedimentary super systems are identified, which are termed S1 and S2, moving from south to north (Fig. 12d; Table 4).

In the southern part of the graben, the cluster of arcuate and lensoidal high amplitude seismic architectures in plan-view, and which display hummocky seismic reflections and down-lapping stepped profiles in cross-section over mid-basin highs (Fig. 11), are interpreted as a reef complex (cf. Fontaine et al., 1987; Wu et al., 2009). The relatively isolated planform distribution of amplitudes, which form as small lenses, reflect several steps in the reef (Fig. 12c) built-up through successive periods of reef-front development. The moderately bright amplitudes

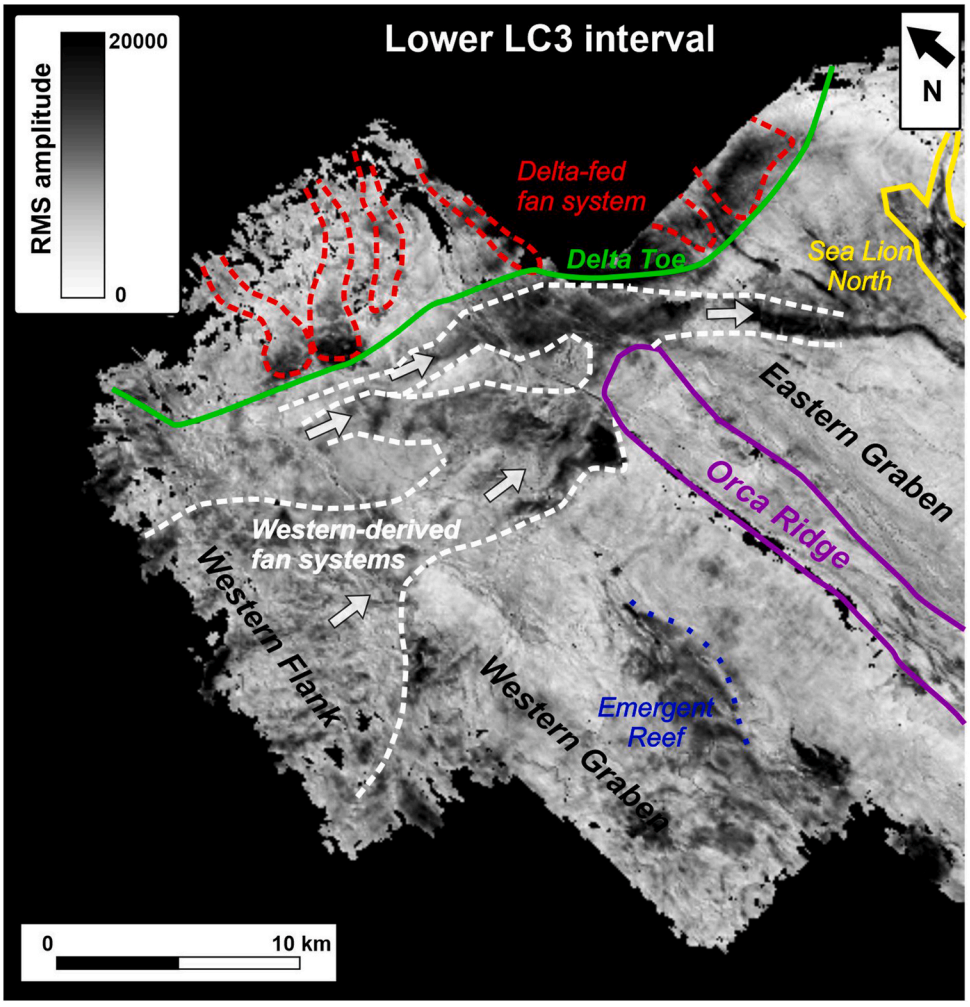

Fig. 10. An RMS amplitude extraction of the Lower LC3 interval across the Western and Eastern grabens. In the north, the higher amplitude features (dark grey to black features on the map) likely represent northerly-derived delta-toe deposits. Immediately south, westerly-derived fan systems appear to flow across the Western Graben, which then pass around the northern extent of the Orca Ridge, draining into the Eastern Graben. In the southern-most part of the study area, a cluster of high amplitude architectures are interpreted to represent possible carbonate reef development. Attribute analysis of seismic data © Falkland Islands Government. All rights reserved.

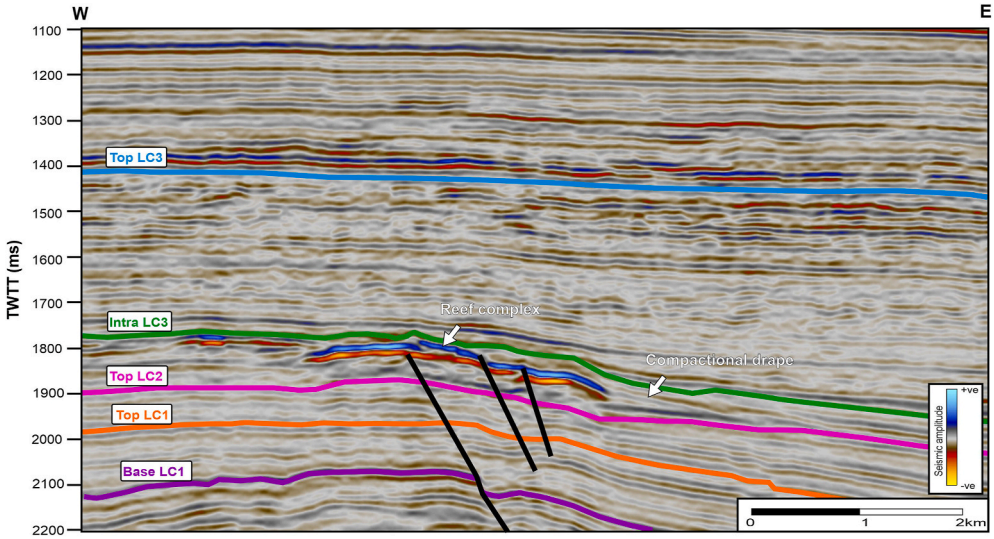

Fig. 11. A W-E interpreted two-way-travel-time seismic crossline, illustrating the potential reef complex shown between 1800 and 1850 ms (see Section 4.5 for more detail). Contains seismic data © Falkland Islands Government. All rights reserved.

flanking the east of the reef are interpreted as reef apron debris (or a reef talus), which is frontally confined against the western edge of the Orca Ridge (Fig. 12d).

It is clear from these observations and interpretations that the intra LC3 horizon marks an important change in depositional processes within the Western Graben. This variability is likely related to a major lowering of lake base level during this time. Consequently, the northern areas were overstepped by deltaic sediments prograding from the north,

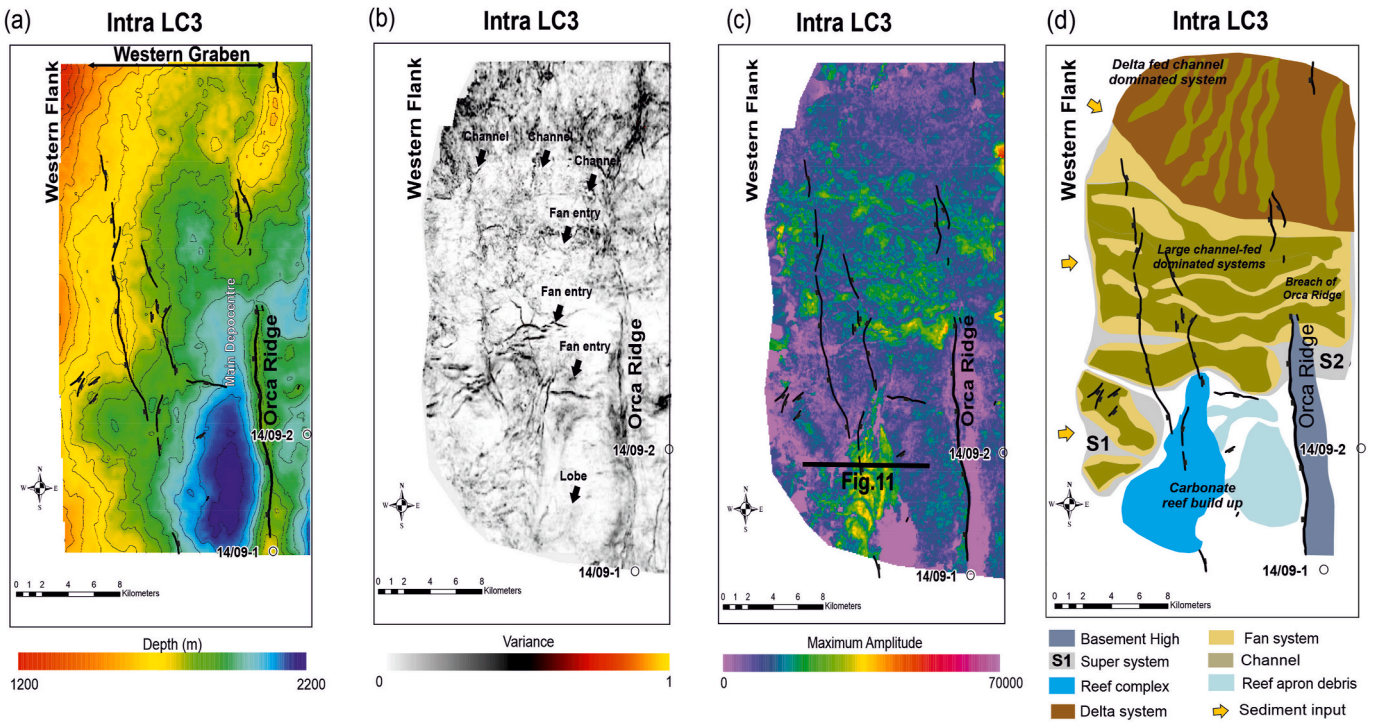

Fig. 12. Seismic characteristics of the Intra LC3 reflector. (a) Structural depth map of the Intra-LC3 horizon, showing one main depocentre. Contours are spaced at 25 m intervals. (b) A variance attribute draped over the Intra-LC3 TWTT horizon. Discontinuities are shown in black, and which highlight the main structural features that intersect this interval. (c) Maximum amplitude extraction map from a 25 msec window around the seismic pick, with zero offset. Brighter colours indicate higher amplitude values, which likely correspond to either sand bodies or fluid changes in the subsurface. Orange polygons represent fan systems, whilst yellow outlines demarcate individual lobe and channels. Light blue and dark blue polygons represent a carbonate reef complex and reef apron debris, respectively. Brown polygons represent an interpreted delta system, which was likely mud-prone with interspersed sandstone-filled channels (represented by yellow polygons). (d) Interpreted seismic facies map of Intra LC3 horizon, showing the super systems, fan systems, lobes, channels, a reef complex, reef apron debris, and a delta system. (For interpretation of the references to colour in this figure legend, the reader is referred to the Web version of this article.)

which began to cover remnant palaeobathymetry on the northern edge of the Orca Ridge (Figs. 4c and 12a). Concomitantly, carbonate reefs were built in the shallow-lacustrine environments along the southern areas of the Western Graben, whilst minor deep-lacustrine fan systems continued to flow from west to east in the deeper areas of the basin.

4.6. Top LC3 (early post-rift)

4.6.1. Description

At the top LC3 interval, the Western Graben forms as a single main depocentre, which is deepest directly adjacent to the Orca Ridge (Fig. 13). The depth of this depocentre varies along strike, with the basal surface at *c.* 2150 m in the south, shallowing-up to *c.* 1900 m in the north (Fig. 13a). The top LC3 package thickens from *c.* 300 m in the north-west to *c.* 700 m in the south (Fig. 4d). In the south, the variance data is relatively continuous, whereas in the north discontinuous low to high sinuosity features are observed (Fig. 13b).

In the north, seismic amplitudes form as a series of north to south or north-east to south-west striking branching networks of sinuous features, which are surrounded by expanses of low seismic amplitude areas (Fig. 13c). The higher amplitude areas widen towards the south, forming a series of broadly south-west to north-east striking architectures, as well as an enigmatic seismically bright shard-like architecture in the south-west (Fig. 13c). At the southernmost part of the Western Graben, there is a distinct change in seismic character from the seismically bright areas to more moderate seismic amplitudes, which display an overall diffuse geometry (Fig. 13d).

4.6.2. Interpretation

The highly sinuous and branching high amplitude features in the north likely represent a network of fluvial channels within a delta-top setting, with the expansive areas of low amplitudes representing associated delta-top mudstones (Fig. 13d). The higher amplitude south-west to north-east striking seismic architectures in the central part of the survey are interpreted as marginal-lacustrine working of coarse-grained delta deposits along palaeo-shorelines. The shard-like high amplitude feature within the higher amplitude areas is interpreted as a relict beach bar system, which was prograded-across and around by the southerly-prograding delta (Fig. 13d). In the southern-most parts of the study area, the change from these high seismic amplitudes to more moderate amplitudes likely represent the southern-most extent of the northerly-derived deltaic system, with the moderate seismic amplitudes interpreted as the distally located shallow-to deep-lacustrine lake areas.

5. Discussion

5.1. Evolution of depositional systems in the Western Graben

During LC1 and LC2, sediment was transported into the Western Graben through a series of broadly W-E striking feeder channels that formed a complex suite of fan systems and stacked lobes in the basin centre (Fig. 14a, b and 14c). These fan systems represent the major sediment transport conduits into the Western Graben during a 'basin-fill phase', which is directly comparable to the 'ponded phase' of Prather et al. (1998). Fan systems formed or active during these phases are typically regarded as sand-rich, although more complex associations have been documented (see Soutter et al., 2019 and references therein). During this phase, the Orca Ridge formed the eastern limit of the Western Graben and acted as a significant barrier or 'sill' (*sensu* Prather et al., 1998) to the depositional systems derived from the Western Flank.

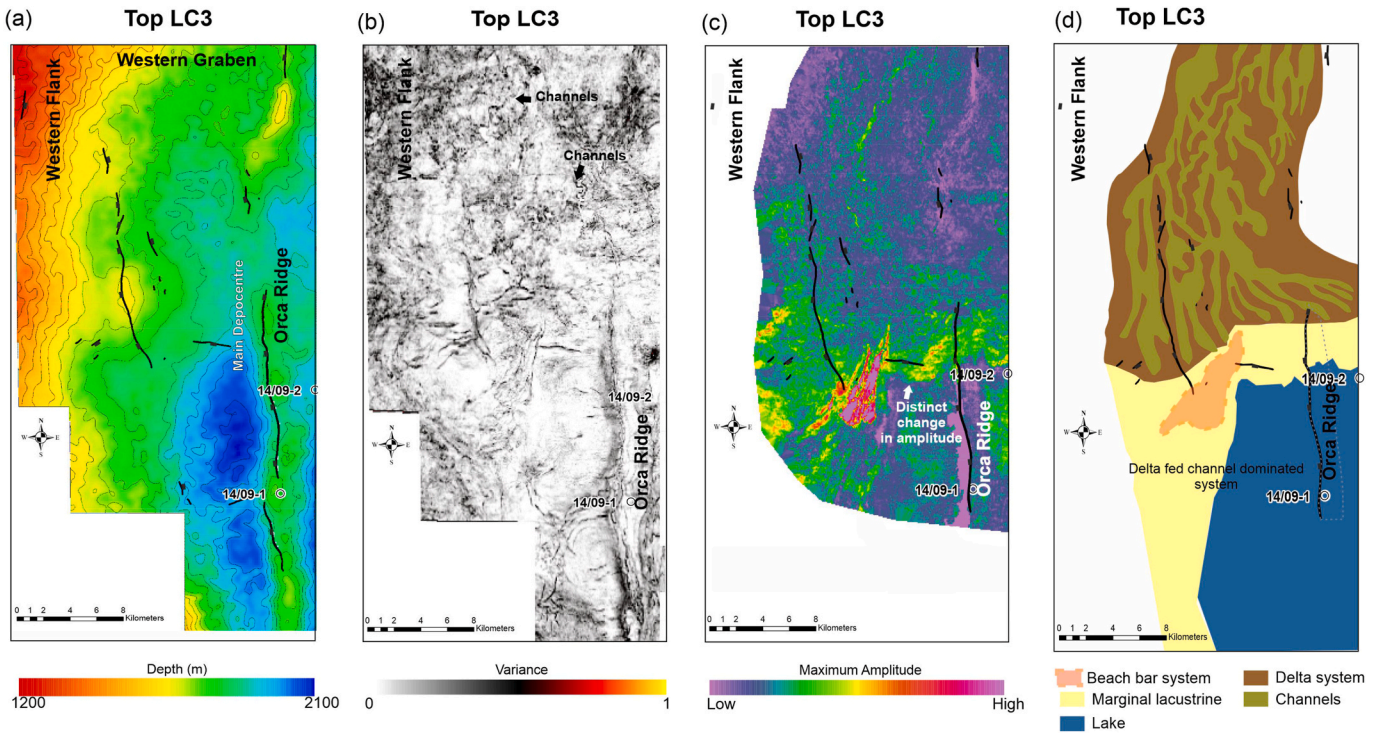

Fig. 13. Seismic characteristics of the Top LC3 interval. (a) A depth-structure map of the Top LC3 horizon, showing one main depocentre. Contours are spaced at 25 m intervals. (b) A variance attribute draped over the Top LC3 horizon, with discontinuities shown in black, highlighting the main structural features that intersect this interval. (c) Maximum amplitude extraction map taken from an interval window between the Top LC3 and Intra-LC3 horizons, with zero offset (on both horizon picks). Brighter colours indicate higher amplitude values that likely correspond to either sand bodies, or fluid changes in the subsurface. Brown polygons represent the extent of interpreted deltaic systems and yellow outlines reflect channels (in this case delta-top channels). Orange polygons represent the presence of a beach bar system. (d) Interpreted seismic facies map of the interval between Top LC3 and Intra-LC3, showing the delta system and internal channels, along with the preserved beach bar systems. (For interpretation of the references to colour in this figure legend, the reader is referred to the Web version of this article.)

This palaeobathymetry caused many of the sedimentary systems to pond adjacent to and along the strike of the Orca Ridge, forming a series of 'frontally-confined' fan systems and fan lobes (Fig. 15a, b, and 15c). Throughout the LC1 interval, the basin represented a fluvio-lacustrine environment at peak highstand, during which time sediments were transported from the Western Flank and into the basin by deep-lacustrine fan systems (Fig. 15a). As sediment supply is intimately linked with water input into lacustrine basins, highstand conditions are thought to represent periods of relatively high sediment supply (Zhang et al., 2019). N–S oriented extensional faults bordered submerged basin highs, causing the LC1 sedimentary systems to be structurally confined, particularly at their lateral margins (off-axis areas). This lateral confinement had a considerable influence on the distribution of the fan systems in the Western Graben, which was further exacerbated by their frontal confinement against the Orca Ridge (Fig. 15a). Sedimentation continued in a similar way during LC2, with a dominant west to east drainage (Fig. 15b). However, a change in fan system/fan distribution is observed in the deep-lacustrine environment between LC1 and LC2 times, and in-particular the location of their lobe-dominated parts of the system. The lobe-dominated areas are comparatively less extensive across western areas of the Western Graben during LC2 times, and instead accumulate predominantly in the east, with longer and more-continuous channel elements feeding the basinally-located lobes (Fig. 14c). This is further supported by an easterly shift in the distribution the thick sedimentary cover between LC1 and LC2 times, which is particularly evident in the southern-most parts of the study area (Fig. 4). This easterly shift in depocenter loci is interpreted to be controlled by a progressive lowering of lake base level and/or inwards shrinking of facies belts associated with the falling stage systems tract, which forced the sedimentary systems eastward.

In LC3 times, northern parts of the Western Graben began to reach the basin fill stage (Fig. 14d and e), during which the northern areas of the Orca Ridge became overtopped and buried by both northerly-derived deltaic sediments and by westerly-derived deep-lacustrine derived fan systems. In early LC3 times, deposition occurred during a period of relatively shallow water, particularly in southern areas, resulting in the formation of a carbonate reef complex in the Western Graben (Figs. 10, 12, 14d and 15c). This carbonate reef complex is positioned over a basin high (Fig. 11) and so likely experienced slightly shallower waters where it was relatively detached from the hinterland siliciclastic drainage systems. Additionally, the network of underlying faults observed in LC2 strata below the reef complex (Fig. 11) may have aided in reef formation through the transportation of basinal nutrient-rich waters to the surface (Fig. 11), which may have enhanced biological productivity in the reef system. Carbonate reef debris aprons formed in down-dip areas to the east of the reef system, where they were frontally confined by the Orca Ridge (Fig. 14d). W-E trending fan systems were confined to basin lows, largely within an area to the north of the carbonate reef complex (Fig. 15c). This is supported by west-east orientated discontinuities in the variance data (Fig. 12b), which indicate that flows incised and potentially by-passed this area during this time. These branching channel elements were able to flow over and through the Orca Ridge, resulting in sediment transport into the Eastern Graben sediment sink (Fig. 10). This suggests that available accommodation space in the Western Graben was diminishing in the more northern areas. The proximity of these flows to the adjacent reef complexes likely resulted in the erosion and redistribution of intraformational carbonate clasts, and their transportation by penecontemporaneous turbidity currents. This relationship is analogous to examples from the Morillo System in the Ainsa Basin (Spanish Pyrenees), where siliciclastic channel fill sediments have been influenced, and to some extent deflected by a nearby carbonate platform along the

Table 1
Sedimentary super systems of Base LC1 (top late syn-rift); descriptions relate to maps shown in Fig. 6.

Super System	Interpretation
S1	Super system (S1) is sourced from the W/WSW. It comprises two flank-fed fan systems, which internally consist of a series of tongue shaped fan lobes (3–4 km in length, 2–3 km in width). The fan lobes are compensationally stacked, shedding sediment into the southern part of depocentre 1, and frontally confined against the western edge of the Orca Ridge.
S2	S2 forms a large W/SW sourced super system, comprising two fan systems that internally consist of large tongue-shaped fan lobes. The southern-most fan system is laterally confined, indicated by two stacked fan lobes. The northern fan system consists of a single fan lobe. Both fan systems are frontally confined against the Orca Ridge and are sourced through a series of gently sinuous to linear feeder channels. Some of the highest amplitudes are observed in the S2 super system.
S3	S3 is partially confined and coalesces with S2. It contains one tongue-shaped fan system that is frontally confined against the Orca Ridge. It is sourced through a network of branching feeders, which were likely fed from a basin-margin canyon system (Fig. 6b). It is likely that the medial part of S2 has been partially influenced or laterally confined by S3, shown by the merging of high amplitudes at fan system limits (Fig. 6c).
S4	S4 consists of one fan system that contains two flank-fed funnel shaped fan lobes sourced by westerly-derived feeder channels. S4 shows some evidence for interaction with both the southerly S3 and the northerly S5. The distal limits of the southern lobe are contained within depocentre 3 and show some evidence for being confined against S3, whilst the northern lobe is frontally confined against the Orca Ridge.
S5	S5 forms the northern-most super system and contains one fan system derived from the NW, forming two elongate fan lobes. The western fan lobe terminates against S4 and coalesces into the feeder system of the eastern fan lobe, whilst the eastern fan lobe by-passes this area and is frontally confined against the Orca Ridge.

high-relief Boltaña Anticline (Bayliss and Pickering, 2015).

The Western Graben evidently experienced a much shallower water setting during early LC3 times, which is directly correlatable to the base LC3 lake lowstand, as observed in the Eastern Graben (Richards and Hillier, 2000; Richards et al., 2006; Dodd et al., 2019). The key control on this lowstand event was likely a combination of semi-regional climate variability (e.g., more arid conditions, leading to decreased sediment transport into the basin centres), and a gradual reduction in available accommodation space as the Western Graben transitioned into the 'fill-phase' regime (*sensu* Prather et al., 1998).

By top LC3 times, the Orca Ridge was buried by sediment, leading to the connection of the Western and Eastern Grabens to form a single continuous basin (Figs. 14d and 15d). Comparisons can be drawn between the fill architecture of the Western Graben and the 'bypass' phase of Prather et al. (1998). The uppermost part of LC3 experienced reduced clastic supply from the west, with the northerly-derived prograding delta system becoming the primary sedimentary system in the Western Graben area during a period of basin highstand (Fig. 15d). This formed a series of delta top deposits in the north of the study area, which transitioned into marginal lacustrine environments in the south. Thesedeposits of which were likely re-worked by littoral processes at the edge of the lake (Figs. 14d and 15e). The shard-like high amplitude feature is interpreted as a beach bar system formed in this marginal-lacustrine setting, which was later overstepped by the southerly prograding delta. The delta brought with it substantial amounts of clastic sediment into the shelf area where the early LC3 reef had previously accumulated, likely resulting in a reduction or termination of carbonate production and subsequent reef abandonment by late LC3 times (Fig. 12c).

5.2. Influence of multi-scale palaeobathymetry on deep-lacustrine fan development

At the broadest scale, the Western Graben represents a ponded basin

Table 2
Super systems of the Top LC1 (rift to sag transition); descriptions relate to maps shown in Fig. 7.

Super System	Interpretation
S1	S1 is composed of two fan systems, with feeder systems deriving sediment from the W/NW. The two fan systems consist of partially confined and laterally confined funnel shaped lobes and are frontally confined by the Orca Ridge (Fig. 7d).
S2	S2 comprises a single large fan system, sourced from the Western Flank. This system consists of two distinct areas of high amplitude, one in the south and one in the north. The southern area is characterised by five tongue-shaped partially confined lobes, which show compensational to aggradational stacking patterns from broadly south-to-north (see Figs. 7d, 8a and 8b). The northern area consists of laterally confined feeder channels and associated lobes that internally display diverse fanning-outwards directions and complex architectural elements. Palaeoflow directions of the northern lobes are interpreted as initially being from west to east, where they are then directed from south-to-north along a terrace formed along a north-south trending basin high, which may have been accompanied by incision into the distal slope (Fig. 7c–d). Subsequently, the flow direction turned ninety degrees towards the east, where the system expanded out and into the less-confined areas of depocentre 1 (Fig. 7a and c).
S3	S3 comprises two fan systems, both sourced from the Western Flank through long elongate feeder channels (6–9 km in length), which coalesce in the southerly low of depocentre 3. Internally, the two fan systems comprise discrete feeder channels attached to down-flow-located east-west oriented elongate lobes, which are frontally confined against the Orca Ridge (Fig. 7d). Incised canyons and channels are observed in variance maps from within the S3 system (Fig. 7b).
S4	S4 comprises sediment drained into depocentre 3 (Fig. 7a) along three main feeder channels that are observed in variance maps (Fig. 7b). These channels coalesce to feed vertically stacked fan lobes deposited, with encircled palaeotopography created in the centre of depocentre 3 (Fig. 7c and d).
S5	S5 comprises two fan systems sourced from both the Western Flank and the north-west. The fan systems are composed of multiple tongue-shaped fan lobes. The western-most fan system appears to terminate against the western margin of the eastern fan system. The eastern fan system forms within depocentre 4 and is frontally confined against the Orca Ridge (Fig. 7d).

Table 3
Sedimentary super systems contemporaneous with the Top LC2 (lower early post-rift); descriptions relate to maps shown in Fig. 9.

Super System	Interpretation
S1	S1 comprises one fan system sourced from the Western Flank, which internally consists of two tongue-shaped fan lobes that are frontally confined by the Orca Ridge (Fig. 9d).
S2	S2 contains three fan systems fed by channels from the Western Flank, which coalesce across the slope forming a series of fan lobes in the basin centre. Medial areas are likely bypassed, with a series of compensationally stacked, partially confined terminal lobes forming distally. These three fan systems are frontally confined by the western edge of the Orca Ridge (Fig. 9d).
S3	S3 contains a complex network of branching and interconnected feeder channels derived from the Western Flank. These feeder channels transition into a series of compensationally stacked fan lobe deposits immediately down-dip of the base of slope, which are frontally confined by the Orca Ridge (Fig. 9d).
S4	S4 is composed of a single fan system, consisting of several north-westerly-derived fan lobes. The southernmost lobe is confined against the northern edge of S3, whilst the other fan lobes are frontally confined against the Orca Ridge (Fig. 9d).

(*sensu* Prather et al., 1998), with internal fan systems sourced from the Western Flank. The ponded basin is confined and contained (*sensu* Southern et al., 2015) throughout LC1 times, with flows unable to surmount mid-basin or basin-edge palaeobathymetry such as the Orca

Table 4
Sedimentary super systems contemporaneous with the Intra LC3 (middle early post-rift); descriptions relate to maps shown in Fig. 12.

Super System	Interpretation
S1	S1 is located west of the reef system and comprises two fan systems: one in the south, which is derived from the south-west and is confined by the western margin of the reef; the other in the north, which is largely derived from the north-west. Both systems contain a single lobe and channel complex (Fig. 12d).
S2	S2 lies directly to the north of the reef and consists of a series of W-E channel-dominated systems. Many of these channels can be mapped over the Orca Ridge and into the Eastern Graben (Fig. 12d).

Ridge (Fig. 15a). This began to change moving into early LC3 times (Fig. 15c), when the Western Graben started to fill with sediment and flows, particularly those in the north were able to travel over the Orca Ridge and into the Eastern Graben (Figs. 10, 12 and 14), forming a 'confined and uncontained basin' (*sensu* Southern et al., 2015) by top LC3 times.

At the super system and fan system scale, fan system distribution and geometries are strongly influenced, and to some extent laterally confined by the effects of intra-basinal palaeobathymetry within the Western Graben. Basin highs bordered by largely N–S oriented faults formed significant palaeobathymetrical features (Fig. 7), which were present during parts of LC1 and throughout LC2, becoming less significant through burial during LC3 times. Their strong influence over fan system geometries is evidenced by the concomitant divergence, deflection, and change in character of seismic architectural elements of the mapped interacting sedimentary systems (Figs. 7 and 9). For example, in the Top LC1 interval of the S2 super system (Fig. 7), palaeobathymetry strongly influenced flow pathways and the resultant architecture of the sedimentary systems. Fan systems were diverted around and along a N–S striking palaeo-high bordered by normal faults (Fig. 15b). This fan system eventually broke through or was able to surmount the palaeobathymetry of the palaeo-high, forming depositional lobes within the westerly-located basin centre. Similar relationships are observed in examples from the Lower Sandstone of the Springar Formation, which dissects the Gjallar Ridge in the Vøring Basin, Norway (Maynard and Gibson, 2001; Southern et al., 2017). Finally, at the super system and fan system scale, all examples from LC1 and LC2 display compelling evidence for frontal confinement and ponding against the Orca Ridge (Figs. 4 and 14), which ultimately controlled the final loci of deposition for each fan system. Frontally confined sedimentary systems are well-known for their thick coarse-grained often tabular clastic sedimentary successions, which are deposited as a consequence of flows being forced to decelerate, and in some cases arrest against a confining slope (Patacci et al., 2014).

When these depositional systems are examined at the lobe and element scale, variations in lobe geometry and stacking pattern architecture are observed. Lateral confinement of lobes is a key feature at the lobe scale. In the example of S2 of the Top LC1 interval (Figs. 7 and 8), the southernmost arm forms within a gap in the Orca Ridge, and the northerly arm is sandwiched between the slope and a linear palaeobathymetrical feature (Fig. 7). The southerly arm is composed of a series of aggradational to compensationally-stacked lobe features that were forced to migrate northwards over time as available accommodation space in the south began to fill with the earliest fan lobe deposits (Fig. 8). In this example, the degree of aggradational lobe stacking within loosely decreases over time, with progressive lobe deposits displaying a higher degree of compensational staking, which can be associated with the gradual in-filling of palaeotopography. Finally, each lobe has been fed by its own feeder channel within the overall fan system (Fig. 7c), suggesting that the infilling of accommodation space in the basin centre, and subsequent potential damming-up of feeder systems of previous lobes may act to force a shift in position of the next feeder system that develops.

5.3. *Variability and evolution of deep-lacustrine fan system type and lobe character*

Within the Western Graben, the deep lacustrine super systems, fan systems, fan lobes, and element-scale geometries show considerable spatial and temporal variability. Structural confinement is observed to exert control on these sedimentary systems, at a range of different scales. When these confined systems are compared with other examples of partial or non-confined (unconfined) deep-lacustrine systems (e.g., the Sea Lion Fan, Dodd et al., 2019; the Beverley Fan, Dodd et al., 2022), the internal character of the fan systems, in particular lobe-scale spatial distribution and stacking patterns, are strongly influenced. These examples provide evidence that deep-lacustrine palaeobathymetry strongly influences the internal sedimentary systems, which requires

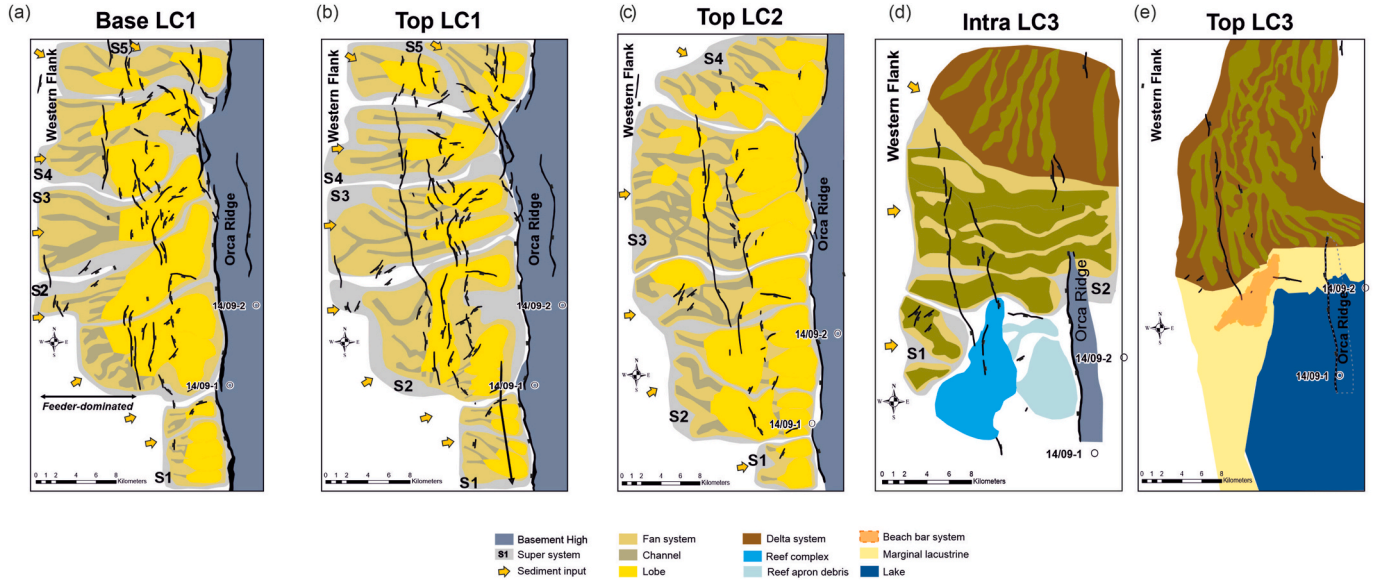

Fig. 14. A summary of interpreted seismic facies maps, and overall palaeogeographical variability within the Western Graben, noted left to right from (a) Base LC1, (b) Top LC1, (c) Top LC2, (d) Intra LC3, and (e)Top LC3.

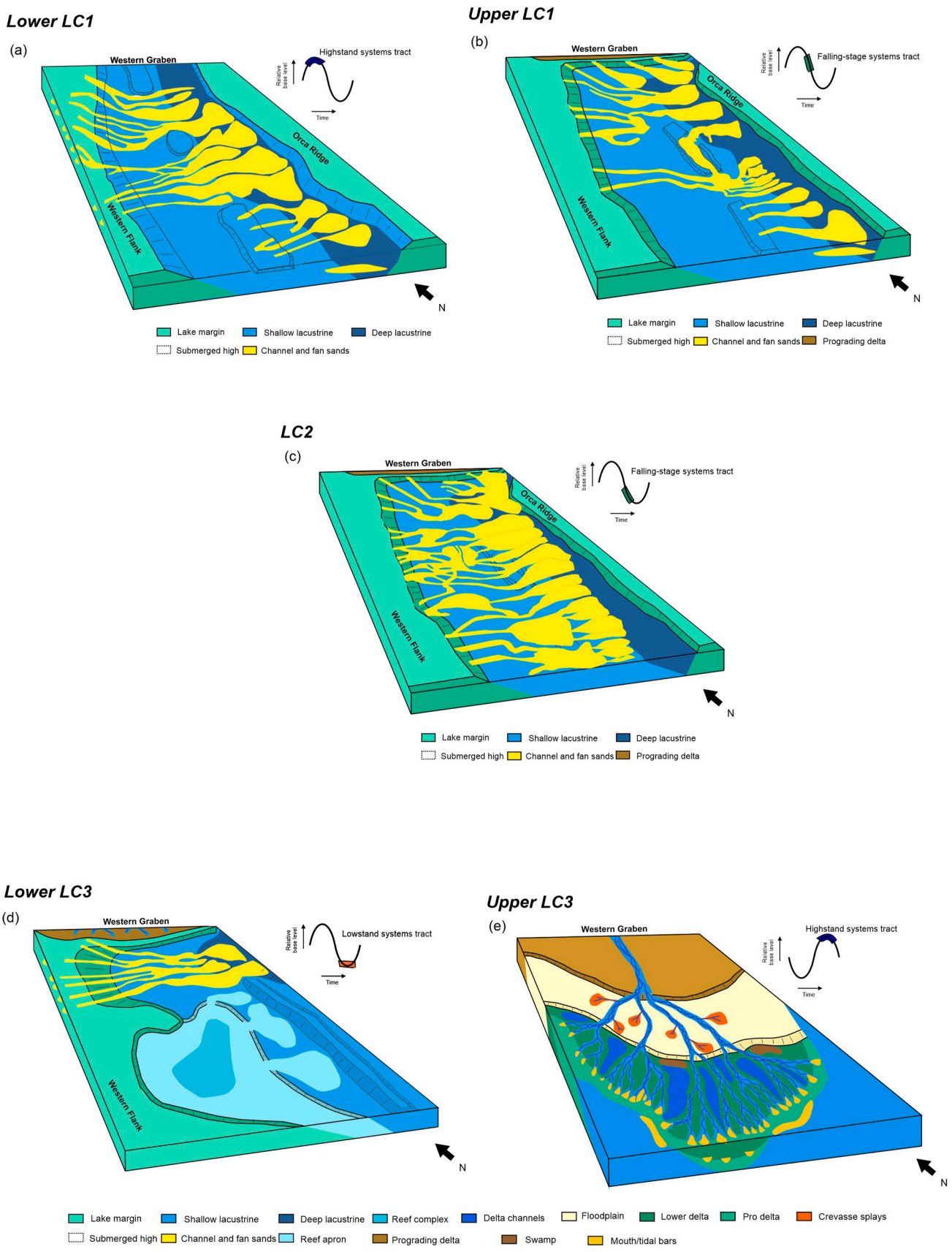

Fig. 15. A series of schematic 3D palaeogeographical models summarising the evolution of the Western Graben throughout the Transitional and Early Post-Rift intervals. Each colour represents different depositional facies environments (see key for details). The relative base level curve illustrates system tracts within the basin evolution. (a) LC1 interval (b) LC2 interval (c) Early LC3 interval. (d) Late LC3 interval. (For interpretation of the references to colour in this figure legend, the reader is referred to the Web version of this article.)

further consideration in the context of deep-lacustrine fan models.

At the lobe scale, one of the key differences between fan systems in the Western Graben and the comparatively less confined examples in the Eastern Graben (i.e., Sea Lion; see Dodd et al., 2019) is a general absence of terminal lobes (terminal splays). This seems to be the case for the frontally confined systems, whose distal-most expression is affected by the Orca Ridge (Fig. 7). Instead of flowing out to their full extent and forming elongate finger-like geometries, these flows were contained within the Western Graben, with their distal-most expressions either redirected laterally along strike of the ridge or reflected in the opposing direction (*sensu* Southern et al., 2015), resulting in flow ponding (Sinclair and Tomasso, 2002 and references therein). In the other examples where these flows were able to surmount the palaeobathymetry, flow stripping likely resulted in a reduction of entrained sediment within the passing flow *(sensu* Sinclair and Tomasso, 2002 and references therein), leaving coarser grained sediments deposited behind the ridge and comparatively lower density finer grained flows passing into the Eastern Graben.

In most areas where fan systems are confined by the Orca Ridge and/or internal palaeobathymetry (Figs. 6, 7 and 9), fan systems and fan lobes are relatively uniform in internal seismic character and generally lack intricate element-scale seismic architectures like those observed in other fan systems such as the Sea Lion, Casper, Zebedee, and Beverley Fan Systems (Dodd et al., 2019, 2022). This is interpreted to suggest the presence of thickly bedded tabular sandstone and mudstone deposits comprising these fan systems and fan lobes. These systems are directly analogous to examples of ponded basins such as the Auger Basin on the central Gulf of Mexico slope (Sinclair and Tomasso, 2002 and references therein). For example, the coalescing lobes of LC2 in the basin centre are frontally confined against the western edge of the Orca Ridge (Fig. 9d). These lobes form directly east and down dip of a series of north-south striking *en-echelon* faults (Fig. 9c), with these fundamentally defining the break in slope and position of the channel-lobe transition zones (CLTZs) in this part of the basin (Fig. 5; Mutti & Normark, 187; Wynn et al., 2002, Brooks et al., 2018 and Dodd et al., 2022). The Orca Ridge provided a significant intra-basinal high during this time, resulting in the frontal confinement of transported sediments, which promoted lobe-scale internal coalescing within these ponded systems and compensational to aggradational stacking patterns.

5.4. Implications for hydrocarbon exploration

In terms of reservoir potential, palaeobathymetricallyinfluenced deep-lacustrine fan systems, and particularly those systems that show evidence for ponding, can deposit and preserve thick and laterally extensive high quality sandstone successions, which typically deposited in the distal and lateral parts of confined basin settings. Ultimately, the scale and type of palaeobathymetrical influence on the sedimentary systems controls' sandstone distribution and reservoir quality in confined deep-lacustrine basin settings.

At the basin scale, confined and contained basins, like that of the Western Graben during LC1 and LC2 times (Figs. 6, 7 and 9), form ponded sheet-like fan systems, particularly along the edges of the basin (Figs. 7 and 9). These fans show alternating high and low seismic amplitude architectures, which suggests the presence of stacked successions of ponded sheet-like sandstones in fan areas (*sensu* Sinclair and Tomasso, 2002) and intervening background hemi-limnic deposits in interfan zones (*sensu* Dodd et al., 2019). However, ponded systems contain thick intra-sequence mudstone caps, which have the potential to form semi-regional baffles to fluid flow (Sinclair and Tomasso, 2002); more-extensive hemi-limnic mudstones potentially form local seals. The frontal confinement and ponding of the fan systems can form an element of stratigraphic closure, with sand potentially trapped behind mid-basin sills. In 'confined and uncontained' basins, such as the Western Graben during LC3 times, basins become uncontained, and flows are able to surmount confining topography and escape the basin. When structural features are surmounted, flow-stripping processes result in a significant proportion of coarse-grained sediment deposited behind the structural features. Subsequently, any sands retained within suspension were potentially deposited in down-flow areas, possibly over the structural high forming a potential trap type. This specific organisation may lead to hydrocarbon potential within post-rift sediments deposited over, and within, structural closures formed directly over intra-basinal structural highs.

At the fan system, fan, and lobe scale, the influence of palaeobathymetry ultimately controls the distribution of potential hydrocarbon reservoir-quality rock types. The fan stacking pattern, which is controlled at least in-part by the type and degree of system confinement, will influence both the spatial and vertical distribution of reservoir quality sandstones in the subsurface. Aggradational and compensationally stacked fan systems and fan lobes may prove to be more attractive drilling targets than offset systems, as fewer wells are required to characterise the former systems than the latter. Finally, at the lobe and element scale, the influence of palaeobathymetry and specifically the ponding of systems can result in more-sheet like deposits that are laterally continuous and less laterally heterogeneous than compared with their unconfined deep-lacustrine counterparts, which have been shown to be highly heterogenous (Dodd et al., 2019, 2022).

6. Conclusions

This study provides an integrated analysis of the transitional and early post-rift sedimentary fill of the Western Graben of the North Falkland Basin. The main structural elements include the Western Flank, Western Graben, and N–S striking Orca Ridge. The Western Flank represents a key sediment source for a series of confined deep-lacustrine fan systems, which were deposited in the Western Graben during transitional LC1 and early post-rift LC2 and LC3 times. A series of super systems, fan systems, lobes, and channel elements within the Western Graben were identified, characterised, and described. Localised palaeobathymetrical features in the Western Graben have influenced the pathways of deep lacustrine fan systems along the slope and in the basin centre. The degree and scale of confinement evolved during basin fill, moving from a confined and contained system where sediment ponded against the Orca Ridge during LC1 and LC2, to a confined and uncontained system where flows were able to escape out of the Western Graben and into the Eastern Graben during LC3. A series of laterally and frontally confined fan systems within the LC1 and LC2 sub-units are recognised, which were sourced through feeder channels that drained into the basin from the Western Flank. The early part of LC3 represents deposition during, and shortly following, a major lowstand event in the basin, which is correlatable to the lowstand surface onto which the Sea Lion fans were deposited in the Eastern Graben. Consequently, during LC3 times the Western Graben experienced a period of low lake levels, with a carbonate reef forming in shallow waters in the south, limited deep-lacustrine fans in the deeper areas to the north of the reef, and the early onset of delta progradation across the study area in the northernmost areas. The Intra LC3 horizon marks a key change in depositional environment in the study area, across which the study areas transitions from a deep-lacustrine basin to a deltaic environment by late LC3 times. Palaeobathymetry is shown to have exerted a strong influence over the distribution of deep-lacustrine fan systems and associated sandstones distribution across the Western Graben. This study demonstrates the effects of confinement on the spatial and temporal distribution, multi-scale character, and individual architectural elements of deep lacustrine fan systems. Understanding the scale and role of palaeobathymetry upon the distribution and character of interacting deep-lacustrine fan systems and fans is important as these basins form important hydrocarbon plays/basins worldwide.

Declaration of competing interest

The authors declare that they have no known competing financial interests or personal relationships that could have appeared to influence the work reported in this paper.

Data availability

Data can be requested from the Department of Mineral Resources, Falkland Island Government

Acknowledgements

Romaine Graham is thanked for her constructive review of this paper. This paper is published by permission of the Director, Department of Mineral Resources, Falkland Islands Government, and the Executive Director, British Geological Survey (UKRI).

References

Adeogba, A.A., McHargue, T.R., Graham, S.A., 2005. Transient fan architecture and depositional controls from near-surface 3-D seismic data, Niger Delta continental slops. AAPG Bull. 89 (5), 627–643. https://doi.org/10.1306/11200404025.

Al Ja'aidi, O.S., McCaffrey, W.D., Kneller, B.C., 2004. Factors influencing the deposit geometry of experimental turbidity currents: implication for sand-body architecture in confined basins. In: Lomas, S.A., Joseph, P. (Eds.), Confined Turbidite Systems, vol. 222. Geological Society London Special Publication, pp. 45–58.

Albertão, G.A., Mulder, T., Eschard, R., 2011. Impact of salt-related palaeotopography on the distribution of turbidite reservoirs: evidence from well-seismic analyses and structural restorations in the Brazilian offshore. Mar. Petrol. Geol. 28 (5), 1023–1046. https://doi.org/10.1016/j.marpetgeo.2010.09.009.

Amy, L.A., Talling, P.J., 2006. Anatomy of turbidites and linked debrites based on long distance (120× 30 km) bed correlation, Marnoso Arenacea Formation, Northern Apennines, Italy. Sedimentology 53 (1), 161–212. https://doi.org/10.1111/j.1365-3091.2005.00756.x.

Amy, L.A., McCaffrey, W.D., Kneller, B.C., 2004. The influence of a lateral basin-slope on the depositional patterns of natural and experimental turbidity currents. In: Lomas, S.A., Joseph, P. (Eds.), 2004. Confined Turbidite Systems. *Geological Society London Special Publications*, pp. 311–330. https://doi.org/10.1144/GSL.SP.2004.221.01.17, 222.

Amy, L.A., Kneller, B.C., McCaffrey, W.D., 2007. Facies architecture of the Grès de Peira Cava, SE France: landward stacking patterns in ponded turbiditic basins. J. Geol. Soc. London 164, 143–162. https://doi.org/10.1144/0016-76492005-019.

As, T.E., Howell, J.A., Janocko, M., Jackson, C.L., 2010. Control of aptian palaeobathymetry on turbidite distribution in the buchan graben, outer moray firth, central north sea. Mar. Petrol. Geol. 27 (2), 412–434. https://doi.org/10.1016/j.marpetgeo.2009.10.014.

Baas, J.H., Van Kesteren, W., Postma, G., 2004. Deposits of depletive high-density turbidity currents: a flume analogue of bed geometry, structure, and texture. Sedimentology 51, 1053–1088. https://doi.org/10.1111/j.1365-3091.2004.00660.x.

Bayliss, N.J., Pickering, K.T., 2015. Deep-marine structurally confined channelised sandy fans: middle eocene Morillo system, Ainsa Basin, Spanish Pyrenees. Earth Sci. Rev. 144, 82–106. https://doi.org/10.1016/j.earscirev.2014.11.014.

Bell, D., Stevenson, C.J., Kane, I.A., Hodgson, D.M., Poyatos-Moré, M., 2018. Topographic controls on the development of contemporaneous but contrasting basin-floor depositional architectures. J. Sediment. Res. 88, 1166–1189. https://doi.org/10.2110/jsr.2018.58.

Bersezio, R., Felletti, F., Riva, S., Micucci, L., 2009. Trends in bed thickness and facies of turbiditic sandstone bodies: unravelling the effects of basin confinement, depositional processes, and modes of sediment supply. Extern. Control Deep-Water Depositional Syst. 92, 303–324.

Booth, J.R., Dean, M.C., DuVernary III, A.E., Styzen, M.J., 2003. Paleo-bathymetric controls on the stratigraphic architecture and reservoir development of confined fans in the Auger Basin: central Gulf of Mexico slope. Mar. Petrol. Geol. 20 (6–8), 563–586. https://doi.org/10.1016/j.marpetgeo.2003.03.008.

Bransden, P.J.E., Burges, P., Durham, M.J., Hall, J.G., 1999. Evidence for multi-phase rifting in the North Falkland Basin. Geol. Soc Geol. Soc., London, Spec. Publ. 153 (1), 425–443. https://doi.org/10.1144/GSL.SP.1999.153.01.26.

Brooks, H., Hogdson, D.M., Brunt, R.L., Peakall, J.P., Hofstra, M., Flint, S., 2018. Deepwater channel-lobe transition zone dynamics: processes and depositional architecture, an example from the Karoo Basin, South Africa. Geol. Soc. Am. Bull. 130, 1723–1746. https://doi.org/10.1130/B31714.1.

Brunt, R.L., Hodgson, D.M., Flint, S.S., Pringle, J.K., Di Celma, C., Prélat, A., Grecula, M., 2013. Confined to unconfined: anatomy of a base of slope succession, Karoo Basin, South Africa. Mar. Petrol. Geol. 41, 206–221. https://doi.org/10.1016/j.marpetgeo.2012.02.007.

Bunt, R.J.W., 2015. The use of seismic attributes for fan and reservoir definition in the Sea Lion Field, North Falkland Basin. Petrol. Geosci. 21, 137–149. https://doi.org/10.1144/petgeo2014-055.

Carvajal, C., Steel, R., 2009. Shelf-edge architecture and bypass of sand to deep water: influence of shelf-edge processes, sea level, and sediment supply. J. Sediment. Res. 79 (9), 652–672. https://doi.org/10.2110/jsr.2009.074.

Chatterjee, P., Kuila, U., Naidu, B.N.S., Bora, H.J., Malkani, A., Dutta, S., Mandal, A., Mishra, P., Mohapatra, P., 2019. Fatehgarh lacustrine turbidite potential, Barmer Baisn, India. Lead. Edge 38 (4), 280–285. https://doi.org/10.1190/tle38040280.1.

Chen, D., Pang, X., Jiang, Z., Zeng, J., Qiu, N., Li, M., 2009. Reservoir characteristics and their effects on hydrocarbon accumulation in lacustrine turbidites in the Jiyang Super-depression, Bohai Bay Basin, China. Mar. Petrol. Geol. 26 (2), 149–162. https://doi.org/10.1016/j.marpetgeo.2008.03.003.

Chen, H., m Zhu, X., Wood, L.J., Shi, R., 2020. Evolution of drainage, sediment-flux and fluvio-delatic sedimentary systems response in hanging wall depocentres in evolving non-marine rift basins: paleogene of Raoyang Sag, Bohai Bay Basin, China. Basin Res. 32 (1), 116–145. https://doi.org/10.1111/bre.12371.

Chopra, S., Marfurt, K.J., 2005. Seismic attributes – a historical perspective. Geophysics 70 (5), 3SO–28S0. https://doi.org/10.1190/1.2098670.

Corella, J.P., Loizeau, J.L., Kremer, K., Hilbe, M., Gerard, J., le Dantec, N., Stark, N., González-Quijano, M., Girardclos, 2016. The role of mass-transport deposits and turbidites in shaping modern lacustrine deepwater channels. Mar. Petrol. Geol. 77, 515–525. https://doi.org/10.1016/j.marpetgeo.2016.07.004.

Covault, J.A., Romans, B.W., 2009. Growth patterns of deep-sea fans revisited: turbidite-system morphology in confined basins, examples from the California Borderland. Mar. Geol. 265 (1–2), 51–66. https://doi.org/10.1016/j.margeo.2009.06.016.

Cunha, R.S., Tinterri, R., Magalhaes, P.M., 2017. Annot Sandstone in the Peïra Cava basin: an example of an asymmetric facies distribution in a confined turbidite system (SE France). Mar. Petrol. Geol. 87, 60–79. https://doi.org/10.1016/j.marpetgeo.2017.04.013.

Davies, C., Haughton, P.D.W., McCaffrey, W., Scott, E., Hogg, N., Kitching, D., 2009. Character and distribution of hybrid sediment gravity flow deposits from the outer Forties Fan, Palaeocene Central North Sea, UKCS. Mar. Petrol. Geol. 26, 1919–1939. https://doi.org/10.1016/j.marpetgeo.2009.02.015.

Dodd, T.J., McCarthy, D.J., Clarke, S.M., 2020. Clastic injectites, internal structures and flow regime during injection: the Sea Lion Injectite System, North Falkland Basin. Sedimentology 67 (2), 1014–1044. https://doi.org/10.1111/sed.12672.

Dodd, T.J.D., McCarthy, D.J., Richards, P.C., 2019. A depositional model for deep-lacustrine, partially confined turbidite fans: early Cretaceous, North Falkland Basin. Sedimentology 66 (1), 53–80. https://doi.org/10.1111/sed.12483.

Dodd, T.J.H., McCarthy, D.J., Amy, L., Plenderleith, G.E., Clarke, S.M., 2022. Hybrid event bed character and distribution in the context of ancient deep-lacustrine fan models. Sedimentology. https://doi.org/10.1111/sed.12979.

Dolson, J., Burley, S.D., Sunder, V.R., Kothari, V., Naidu, B., Whiteley, N.P., Farrimond, P., Taylor, A., Direen, N., Ananthakrishnan, B., 2015. The discovery of the Barmer Basin, Rajasthan, India, and its petroleum geology. AAPG (Am. Assoc. Pet. Geol.) Bull. 99 (3), 433–465. https://doi.org/10.1306/10021414045.

Dorrell, R.M., Patacci, M., McCaffrey, W.D., 2018. Inflation of ponded, particulate laden density currents. J. Sediment. Res. 88, 1276–1282. https://doi.org/10.2110/jsr.2018.65.

Drinkwater, N.J., Pickering, K.T., 2001. Architectural elements in a high-continuity sand-prone turbidite system, late precambrian kongsfjord formation, northern Norway: application to hydrocarbon reservoir characterization. AAPG (Am. Assoc. Pet. Geol.) Bull. 85 (10), 1731–1757. https://doi.org/10.1306/8626D059-173B-11D7-8645000102C1865D.

Etienne, S., Mulder, T., Bez, M., Desaubliaux, G., Kwasniewski, A., Parize, O., Dujoncquoy, E., Salles, T., 2012. Multiple scale characterization of sand-rich distal lobe deposit variability: examples from the Annot Sandstones Formation, Eocene-Oligocene, SE France. Sediment. Geol. 273, 1–18. https://doi.org/10.1016/j.sedgeo.2012.05.003.

Fallgatter, C., Buso, V.V., Paim, O.S.G., Milana, J.P., 2019. Stratigraphy and depositional architecture of lobe complexes across a range of confinements: examples from the Late Paleozoic Panganzo Basin, Argentina. Mar. Petrol. Geol. 110, 254–274. https://doi.org/10.1016/j.marpetgeo.2019.07.020.

Farfour, M., Ferahtia, J., Djarfour, N., Aitouch, M.A., 2017. Seismic spectral decomposition applications in seismic. A review and application. In: Gaci, S., Hachay, O. (Eds.), Oil and Gas Exploration. https://doi.org/10.1002/9781119227519.ch6.

Fildani, A., Normark, W.R., 2004. Late Quaternary evolution of channel and lobe complexes of Monterey Fan. Mar. Geol. 206 (1–4), 199–223. https://doi.org/10.1016/j.margeo.2004.03.001.

Fonnesu, M., Patacci, M., Haughton, P.D.W., Felletti, F., McCaffrey, W.D., 2016. Hybrid event beds generated by local substrate delamination on a confined-basin floor. J. Sediment. Res. 86 (8), 929–943. https://doi.org/10.2110/jsr.2016.58.

Fonnesu, M., Felletti, F., Haughton, P.D.W., Patacci, M., McCaffrey, W.D., 2018. Hybrid event bed character and distribution linked to turbidite system sub-enviornments: the North Apennine Gottero Sandstone (north-west Italy). Sedimentology 65, 151–190. https://doi.org/10.1111/sed.12376.

Fontaine, J.M., Cussey, R., Lacaze, J., Lanaud, R., Yapaudjian, L., 1987. Seismic interpretation of carbonate depositional environments. AAPG bulletin 71 (3), 281–297. https://doi.org/10.1306/94886E7F-1704-11D7-8645000102C1865D.

Francis, A., Lewis, M., Booth, C., 2015. Sea Lion field, North Falkland basin: seismic inversion and quantitative interpretation. Petrol. Geosci. 21 (2–3), 151–169. https://doi.org/10.1144/petgeo2014-048.

Gardiner, A.R., 2006. The variability of turbidite sandbody pinchout and its impact on hydrocarbon recovery in stratigraphically trapped fields. Geol. Soc. London, Spec. Publ. 254, 267–287. https://doi.org/10.1144/GSL.SP.2006.254.01.14.

Gawthorpe, R.L., Leeder, M.R., 2000. Tectono-sedimentary evolution of active extensional basins. Basin Res. 12 (3–4), 195–218. https://doi.org/10.1111/j.1365-2117.2000.00121.x.

Gervais, A., Savoye, B., Piper, D.J.W., Mulder, T., Cremer, M., Pichevin, L., 2004. Present Morphology and Depositional Architecture of a Sandy Confined Submarine System: the Golo Turbidite System (Eastern Margin of Corsica), vol. 222. Geological Society London Special Publications, pp. 59–89. https://doi.org/10.1144/GSL.SP.2004.222.01.05.

Hamilton, P., Gaillot, G., Strom, K., Fedele, J., Hoyal, D., 2017. Linking hydraulic properties in supercritical submarine distributary channels to depositional-lobe geometry. J. Sediment. Res. 87 (9), 935–950. https://doi.org/10.2110/jsr.2017.53.

Hansen, L., Janocko, M., Kane, I., Kneller, B., 2017. Submarine channel evolution, terrace development, and preservation of intra-channel thin-bedded turbidites: mahin and Avon channels, offshore Nigeria. Mar. Geol. 383, 146–167. https://doi.org/10.1016/j.margeo.2016.11.011.

Haughton, P.D.W., 2000. Evolving turbidite systems on a deforming basin flow, Tabernas, SE Spain. Sedimentology 47 (3), 497–518. https://doi.org/10.1046/j.1365-3091.2000.00293.x.

Haughton, P.D.W., Barker, S.P., McCaffrey, W.D., 2003. 'Linked' debrites in sand-rich turbidite systems–origin and significance. Sedimentology 50 (3), 459–482. https://doi.org/10.1046/j.1365-3091.2003.00560.x.

Haughton, P., Davis, C., McCaffrey, W., Barker, S., 2009. Hybrid sediment gravity flow deposits — classification, origin, and significance. Mar. Petrol. Geol. 26, 1900–1918. https://doi.org/10.1016/j.marpetgeo.2009.02.012.

Hodgson, D.M., 2009. Distribution and origin of hybrid beds in sand-rich submarine fans of the Tanqua depocentre, Karoo Basin, South Africa. Mar. Petrol. Geol. 26 (10), 1940–1956. https://doi.org/10.1016/j.marpetgeo.2009.02.011.

Hodgson, D.M., Haughton, P.D.W., 2004. Impact of Syndepositional Faulting on Gravity Current Behaviour and Deep-Water Stratigraphy: Tabernas-Sorbas Basin, vol. 222. *Geological Society of London Special Publications*, SE Spain, pp. 135–158. https://doi.org/10.1144/GSL.SP.2004.222.01.08.

Jobe, Z.R., Sylvester, Z., Howes, N., Pirmez, C., Parker, A., Cantelli, A., Smith, R., Wolinksy, M.A., O'Byrne, C., Slowey, N., Prather, B., 2017. High-resolution, millennial-scale patterns of bed compensation on a sand-rich intraslope submarine fan, western Niger Delta slope. GSA Bulletin 129 (1–2), 23–37. https://doi.org/10.1130/B31440.1.

Jones, D.J.R., McCarthy, D.J., Dodd, T.J.D., 2019. Tectonostratigraphy and the petroleum systems in the Northern sector of the North Falkland Basin, south atlantic. Mar. Petrol. Geol. 103, 150–162. https://doi.org/10.1016/j.marpetgeo.2019.02.020.

Kane, I.A., Catterall, V., McCaffrey, W.D., Martinsen, O.J., 2010. Submarine channel response to intrabasinal tectonics: the influence of lateral tilt. AAPG (Am. Assoc. Pet. Geol.) Bull. 94 (2), 189–219. https://doi.org/10.1306/08180909059.

Kneller, B., McCaffrey, W., 1999. Depositional effects of flow nonuniformity and stratification within turbidite currents approaching a bounding slope; deflection, reflection, and facies variation. J. Sediment. Res. 69 (95), 980–991. https://doi.org/10.2110/jsr.69.980.

Lee, H.H., Watkins, J.S., Bryant, W.R., 1996. Bryant Canyon fan system: an unconfined, large river-sourced systems in the northwestern Gulf of Mexico. AAPG (Am. Assoc. Pet. Geol.) Bull. 80 (3), 340–357. https://doi.org/10.1306/64ED87DC-1724-11D7-8645000102C1865D.

Li, L., Wang, Y., Zhang, L., Huang, Z., 2010. Confined gravity flow sedimentary process and its impact on the lower continental slope, Niger Delta. Sci. China Earth Sci. 53, 1169–1175. https://doi.org/10.1007/s11430-010-4018-8.

Li, L., Jiang, Z., Liu, K., Zhang, C., You, X., 2014. Factors controlling reservoir properties and hydrocarbon accumulation of lacustrine deep-water turbidites in the Huimin Depression, Bohai Bay Basin, East China. Mar. Petrol. Geol. 57, 327–344. https://doi.org/10.1016/j.marpetgeo.2014.06.007.

Lohr, T., Underhill, J., 2015. Role of rift transection and punctuated subsidence in the development of the North Falkland Basin. Petrol. Geosci. 21, 85–110. https://doi.org/10.1144/petgeo2014-050.

Lomas, S.A., Joseph, P., 2004. Confined turbidite systems. In: Lomas, S.A., Joseph, P. (Eds.), 2004. Confined Turbidite Systems. *Geological Society London Special Publications*, pp. 1–7. https://doi.org/10.1144/GSL.SP.2004.222.01.01, 222.

MacAulay, F., 2015. Sea Lion field discovery and appraisal; a turning point for the north Falkland Basin. Petrol. Geosci. 21, 111–124. https://doi.org/10.1144/petgeo2014-044.

Marini, M., Milli, S., Ravnås, R., Moscatelli, M., 2015. A comparative study of confined vs. semi-confined turbidite lobes from the Lower Messinian Laga Basin (Central Apennines, Italy): implications for assessment of reservoir architecture. Mar. Petrol. Geol. 63, 142–165. https://doi.org/10.1016/j.marpetgeo.2015.02.015.

Marini, M., Patacci, M., Felletti, F., McCaffrey, W.D., 2016a. Fill to spill stratigraphic evolution of a confined turbidite mini-basin succession, and its likely well bore expression: the Castagnola Fm, NW Italy. Mar. Petrol. Geol. 69, 94–111. https://doi.org/10.1016/j.marpetgeo.2015.10.014.

Marini, M., Felletti, F., Milli, S., Patacci, M., 2016b. The thick-bedded tail of turbidite thickness distribution as a proxy for flow confinement: examples from tertiary basins of central and northern Apennines (Italy). Sediment. Geol. 34, 96–118. https://doi.org/10.1016/j.sedgeo.2016.05.006.

Maynard, J.R., Gibson, J.P., 2001. Potential for subtle traps in the permian rotliegend of the UK Southern North sea. Petrol. Geosci. 7 (3), 301–314. https://doi.org/10.1144/petgeo.7.3.301.

McCaffrey, W., Kneller, B., 2001. Process controls on the development of stratigraphic trap potential on the margins of confined turbidite systems and aid to reservoir evaluation. AAPG (Am. Assoc. Pet. Geol.) Bull. 85 (6), 971–988. https://doi.org/10.1306/8626CA41-173B-11D7-8645000102C1865D.

McCarthy, D., Aldiss, D., Arsenikos, S., Stone, P., Richards, P., 2017. Comment on "Geophysical evidence for a large impact structure on the Falkland (Malvinas) Plateau. Terra Nova 29 (6), 411–415.

McHargue, T., Pyrcz, M.J., Sullivan, M.D., Clark, J.D., Fildani, A., Romans, B.W., Covault, J.A., Levy, M., Posamentier, H.W., Drinkwater, N.J., 2011. Architecture of turbidite channel systems on the continental slope: patterns and predictions. Mar. Petrol. Geol. 28 (3), 728–743. https://doi.org/10.1016/j.marpetgeo.2010.07.008.

Moscardelli, L., Wood, L.J., Dunlap, D.B., 2012. Shelf-edge deltas along structurally complex margins: a case study from eastern offshore Trinidad. AAPG (Am. Assoc. Pet. Geol.) Bull. 96 (8), 1483–1522. https://doi.org/10.1306/01241211046.

Mutti, E., Normark, W.R., 1987. Comparing examples of modern and ancient turbidite systems: problems and concepts. In: Leggett, J.K., Zuffa, G.G. (Eds.), Marine Clastic Sedimentology. Springer, Dordrecht, the Netherlands, pp. 1–38. https://doi.org/10.1007/978-94-009-3241-8_1.

Mutti, E., Bernoulli, D., Lucchi, F.R., Tinterri, R., 2009. Turbidites and turbidity currents from Alpine 'flysch' to the exploration of continental margins. Sedimentology 56 (1), 267–318. https://doi.org/10.1111/j.1365-3091.2008.01019.x.

Normark, W.R., Posamentier, H., Mutti, E., 1993. Turbidite systems; state of the art and future directions. Rev. Geophys. 31 (2), 91–116. https://doi.org/10.1029/93RG02832.

Oluboyo, A.P., Gawthorpe, R.L., Bakke, K., Hadler-Jacobsen, F., 2014. Salt tectonic controls on deep-water turbidite depositional systems: miocene, southwestern Lower Congo Basin, offshore Angola. Basin Res. 26 (4), 597–620. https://doi.org/10.1111/bre.12051.

Patacci, M., Haughton, P.D.W., McCaffrey, W.D., 2014. Rheological complexity in sediment gravity flows forced to decelerate against a confining slope, Braux, SE France. J. Sediment. Res. 84, 270–277. 10.2110/jsr.2014.26.

Patacci, M., Marini, M., Felletti, F., Di Giulio, A., Setti, M., McCaffrey, W.D., 2020. Origin of mud in turbidites and hybrid event beds: insight from ponded mudstone caps of the Castagnola turbidite system (north-west Italy). Sedimentology 67 (5), 2625–2644. https://doi.org/10.1111/sed.12713.

Pickering, K.T., Hilton, V.C., 1998. Turbidite Systems of Southeast France: Application to Hydrocarbon Prospectivity. Vallis Press.

Pickering, K.T., Underwood, M.B., Taira, A., 1992. Open-ocean to trench turbidity-current flow in the Nankai Trough: flow collapse and reflection. Geology 20 (12), 1099–1102. https://doi.org/10.1130/0091-7613(1992)020<1099:OOTTTC>2.3.CO;2.

Plenderleith, G.E., Dodd, T.J.H., McCarthy, D.J., 2022. The effect of breached relay ramp structures on deep-lacustrine sedimentary systems. Basin Res. https://doi.org/10.1111/bre.12655.

Posamentier, H.W., Kolla, K., 2003. Seismic geomorphology and stratigraphy of depositional elements in deep-water settings. J. Sediment. Res. 73 (3), 367–388. https://doi.org/10.1306/111302730367.

Prather, B.E., 2003. Controls on reservoir distribution, architecture, and stratigraphic trapping in slope settings. Mar. Petrol. Geol. 20 (6–8), 529–545. https://doi.org/10.1016/j.marpetgeo.2003.03.009.

Prather, B.E., Booth, J.R., Steffens, G.S., Craig, P.A., 1998. Classification, lithologic calibration, and stratigraphic succession of seismic facies of intraslope basins, deep-water Gulf of Mexico. AAPG (Am. Assoc. Pet. Geol.) Bull. 82 (5A), 701–728.

Ravnas, R., Steel, R.J., 1998. Architecture of marine rift-basin successions. AAPG (Am. Assoc. Pet. Geol.) Bull. 82, 110–146. https://doi.org/10.1306/1D9BC3A9-172D-11D7-8645000102C1865D.

Richards, P.C., Fannin, N.G.T., 1997. Geology of the north Falkland Basin. J. Petrol. Geol. 20 (2), 165–183. https://doi.org/10.1111/j.1747-5457.1997.tb00771.x.

Richards, P.C., Hillier, B.V., 2000. Post-drilling analysis of the north Falkland Basin – Part 1. Tectono-stratigraphic framework. J. Petrol. Geol. 23 (3), 253–272. https://doi.org/10.1111/j.1747-5457.2000.tb01019.x.

Richards, P.C., Gatliff, R.W., Quinn, M.F., Fannin, N.G.T., 1996a. Petroleum potential of the Falkland Islands offshore areas. J. Petrol. Geol. 19 (2), 161–182. https://doi.org/10.1111/j.1747-5457.1996.tb00423.x.

Richards, P.C., Gatliff, R.W., Quinn, M.F., Williamson, J.P., Fannin, N.G.T., 1996b. The geological evolution of the Falkland Islands continental shelf. From Storey. B.C. In: King, E.C., Livermore, R.A. (Eds.), 1996, Weddell Sea Tectonics and Gondwana Break-Up. Geological Society Special Publication, pp. 105–128. https://doi.org/10.1144/GSL.SP.1996.108.01.08, 108.

Richards, P., Duncan, I., Phipps, C., Pickering, G., Grzywacz, J., Hoult, R., Merrit, J., 2006. Exploring for fan and delta sandstones in the offshore Falkland Basins. J. Petrol. Geol. 29 (3), 199–214. https://doi.org/10.1111/j.1747-5457.2006.00199.x.

Richardson, N.J., Underhill, J.R., 2002. Controls on the structural architecture and sedimentary character of syn-rift sequences, North Falkland Basin, South Atlantic. Mar. Petrol. Geol. 19 (4), 417–443. https://doi.org/10.1016/S0264-8172(02)00024-7.

Sandwell, D.T., Müller, R.D., Smith, W.H., Garcia, E., Francis, R., 2014. New global marine gravity model from CryoSat-2 and Jason-1 reveals buried tectonic structure. science 346 (6205), 65–67. https://doi.org/10.1126/science.1258213.

Scholz, C., Rosendahl, B.R., Scott, D.L., 1990. Development of coarse-grained facies in lacustrine rift basins: examples from East Africa. Geology 18 (2), 140–144. https://doi.org/10.1130/0091-7613(1990)018<0140:DOCGFI>2.3.CO;2.

Shanmugam, G., Moiola, R.J., 1988. Submarine fans: characteristics, models, classification, and reservoir potential. Earth Sci. Rev. 24 (6), 383–428. https://doi.org/10.1016/0012-8252(88)90064-5.

Simpson, J.E., 1987. Gravity Currents: in the Environment and the Laboratory, *second ed.* Cambridge University Press, p. 244. https://doi.org/10.1017/S001675689861150X.

Sinclair, H.D., 2000. Delta-fed turbidites infilling topographically complex basins: a new depositional model for the Annot Sandstones, SE France. J. Sediment. Res. 70 (3), 504–519. https://doi.org/10.1306/2DC40923-0E47-11D7-8643000102C1865D.
Sinclair, H.D., Tomasso, M., 2002. Depositional evolution of confined turbidite basins. J. Sediment. Res. 72 (4), 451–456. https://doi.org/10.1306/111501720451.
Smith, R.D.A., 1995. Reservoir Architecture of Syn-Rift Lacustrine Turbidite Systems, Early Cretaceous, Offshore South Gabon, vol. 80. Geological Society London Special Publications, pp. 197–210. https://doi.org/10.1144/GSL.SP.1995.080.01.10.
Smith, R.D.A., Joseph, P., 2004. Deep-water sedimentation in the Alpine basin of SE France: new perspectives on the Grès d'Annot and related systems. Geol. Soc. London 221, 1–16. https://doi.org/10.1144/GSL.SP.2004.221.01.01.
Soreghan, M.J., Scholz, C.A., Wells, J.T., 1999. Coarse-grained, deep-water sedimentation along a border fault margin of Lake Malawi, Africa; seismic stratigraphic analysis. J. Sediment. Res. 69 (4), 832–846. https://doi.org/10.2110/jsr.69.832.
Southern, S.J., Mountney, N.P., Pringle, J.K., 2014. The carboniferous southern Pennine Basin. UK Geol. Today 30 (2), 71–78. https://doi.org/10.1111/gto.12044.
Southern, S.J., Patacci, M., Felletti, F., McCaffrey, W.D., 2015. Influence of flow containment and substrate entrainment upon sandy hybrid event beds containing a co-genetic mud-clast-rich division. Sediment. Geol. 321, 105–122. https://doi.org/10.1016/j.sedgeo.2015.03.006.
Southern, S.J., Kane, I.A., Warchol, J., Porten, K.W., McCaffrey, W.D., 2017. Hybrid event beds dominated by transitional-flow facies: character, distribution and significance in the Maastrichtian Springar Formation, north-west Vøring Basin, Norwegian Sea. Sedimentology 64 (3), 747–776. https://doi.org/10.1111/sed.12323.
Soutter, E.L., Kane, I.A., Fuhrmann, A., Cumberpatch, Z.A., Huuse, M., 2019. The stratigraphic evolution of onlap in siliciclastic deep-water systems: autogenic modulation of allogenic signals. J. Sediment. Res. 89, 890–917.
Soutter, E.L., Bell, D., Cumberpatch, Z.A., Ferguson, R.A., Spychala, Y.T., Kane, I.A., Eggenhuisen, J.T., 2021. The influence of confining topography orientation on experimental turbidity currents and geological implications. Front. Earth Sci. 8, 540633.
Spychala, Y.T., Hodgson, D.M., Stevenson, C.J., Flint, S., 2017. Aggradational lobe fringes: the influence of subtle intrabasinal seabed topography on sediment gravity flow processes and lobe stacking patterns. Sedimentology 64, 582–608. https://doi.org/10.1111/sed.12315.
Stanca, R.M., Paton, D.A., Hodgson, D.M., McCarthy, D.J., Mortimer, E.M., 2019. A revised position for the rotated Falkland Islands microplate. J. Geol. Soc. 176, 417–429. https://doi.org/10.1144/jgs2018-163.
Stow, D.A.V., Johansson, M., 2000. Deep-water massive sands: nature, origin, and hydrocarbon implications. Mar. Petrol. Geol. 17 (2), 145–174. https://doi.org/10.1016/S0264-8172(99)00051-3.
Straub, K.M., Pyles, D.R., 2012. Quantifying the hierarchical organization of compensation in submarine fans using surface statistics. J. Sediment. Res. 82 (11), 889–898. https://doi.org/10.2110/jsr.2012.73.
Sun, N., Zhong, J., Hao, B., Ge, Y., Swennen, R., 2020. Sedimentological and diagenetic control on the reservoir quality of deep-lacustrine sedimentary gravity flow sand reservoirs of the Upper Triassic Yanchang Formation in Southern Ordos Basin, China. Mar. Petrol. Geol. 112, 104050 https://doi.org/10.1016/j.marpetgeo.2019.104050.
Tagliaferri, A., Tinterri, R., Pontiggia, M., Da Pra, A., Davoli, G., Bonamini, E., 2018. Basin-scale, high-resolution three-dimensional facies modelling of tectonically confined turbidites: an example from the Firenzuola system (Marnoso-arenacea Formation, northern Apennines, Italy). AAPG (Am. Assoc. Pet. Geol.) Bull. 102 (8), 1601–1626. https://doi.org/10.1306/12081716521.
Talling, P.J., 2013. Hybrid submarine flows comprising turbidity current and cohesive debris flow: deposits, theoretical and experimental analyses, and generalized models. Geosphere 9 (3), 460–488.
Terlaky, V., Arnott, R.W.C., 2016. The control of terminal-splay sedimentation on depositional patterns and stratigraphic evolution in avulsion-dominated, unconfined, deep-marine basin-floor systems. J. Sediment. Res. 86 (7), 786–799. https://doi.org/10.2110/jsr.2016.51.
Tinterri, R., Tagliaferri, A., 2015. The syntectonic evolution of foredeep turbidites related to basin segmentation: facies response to the increase in tectonic confinement (Marnoso-arenacea Formation, Miocene, Northern Apennines, Italy). Mar. Petrol. Geol. 67, 81–110. https://doi.org/10.1016/j.marpetgeo.2015.04.006.
Tokes, L., Patacci, M., 2018. Quantifying tabularity of turbidite beds and its relationship to the inferred degree of basin confinement. Mar. Petrol. Geol. 87, 659–671. https://doi.org/10.1016/j.marpetgeo.2018.06.012.
Williams, L.S., 2015. Sedimentology of the lower cretaceous reservoirs of the Sea Lion field, North Falkland basin. Petrol. Geosci. 21 (2–3), 183–198. https://doi.org/10.1144/petgeo2014-039.
Winker, C.D., 1996. High-Resolution seismic stratigraphy of a late pleistocene submarine fan ponded by salt-withdrawal mini-basins on the Gulf of Mexico continental slope. In: Offshore Technology Conference 8024, 6–9th May 1996. https://doi.org/10.4043/8024-MS. Houston, Texas, USA.
Wu, S., Yuan, S., Zhang, G., Ma, Y., Mi, L., Xu, N., 2009. Seismic characteristics of a reef carbonate reservoir and implications for hydrocarbon exploration in deepwater of the Qiongdongnan Basin, northern South China Sea. Marine and Petroleum Geology 26 (6), 817–823. https://doi.org/10.1016/j.marpetgeo.2008.04.008.
Wynn, R.B., Kenyon, N.H., Masson, D.G., Stow, D.A.V., Weave, P.P.E., 2002. Characterization and recognition of deep-water channel-lobe transition zones. AAPG (Am. Assoc. Pet. Geol.) Bull. 86, 1441–1462. https://doi.org/10.1306/61EEDCC4-173E-11D7-8645000102C1865D.
Xian, B., Wang, J., Gong, C., Yin, Y., Chao, C., Liu, J., Zhang, G., Yan, Q., 2018. Classification and sedimentary characteristics of lacustrine hyperpycnal channels: triassic outcrops in the south Ordos Basin, central China. Sediment. Geol. 368, 68–82. https://doi.org/10.1016/j.sedgeo.2018.03.006.
Xu, S., Cong, F., Hao, F., Xu, C., Zou, H., Zhang, X., Xu, S., 2018. Shelf-edge trajectory and sediment dispersal in a lacustrine setting: a case study from Qinnan Depression, Bohai Bay Basin, China. Mar. Petrol. Geol. 91, 562–575. https://doi.org/10.1016/j.marpetgeo.2018.01.027.
Yan, S.Y., Kim, J.W., 2014. Pliocene basin-floor fan sedimentation in the Bay of Bengal (offshore northwest Myanmar). Mar. Petrol. Geol. 49, 45–58. https://doi.org/10.1016/j.marpetgeo.2013.09.007.
Zhang, X., Schola, C.A., 2015. Turbidite systems of lacustrine rift basins: examples from the lake kivu and lake albert rifts, east africa. Sediment. Geol. 325, 177–191. https://doi.org/10.1016/j.sedgeo.2015.06.003.
Zhang, J., Shenghe, W., Wang, X., Lin, Y., Fan, H., Jiang, L., Wan, Q., Yin, H., Lu, Y., 2015. Reservoir quality variations within a sinuous deep water channel system in the Niger Delta Basin, offshore West Africa. Mar. Petrol. Geol. 63, 166–188. https://doi.org/10.1016/j.marpetgeo.2015.02.041.
Zhang, J., Olariu, C., Steel, R., Kim, W., 2019. Climatically controlled lacustrine clinoforms: theory and modelling results. Basin Res. Spec. Issue Article 32, 240–250. https://doi.org/10.1111/bre.12383.